Coherent excitation transport through ring-shaped networks

Francesco Perciavalle^{1,2}, Oliver Morsch³, Davide Rossini², and Luigi Amico^{1,4,5,6}

¹Quantum Research Center, Technology Innovation Institute, P.O. Box 9639 Abu Dhabi, UAE

²Dipartimento di Fisica dell'Università di Pisa and INFN, Largo Pontecorvo 3, I-56127 Pisa, Italy

³CNR-INO and Dipartimento di Fisica dell'Università di Pisa, Largo Pontecorvo 3, 56127 Pisa, Italy

⁴Dipartimento di Fisica e Astronomia, Via S. Sofia 64, 95127 Catania, Italy ⁵INFN-Sezione di Catania, Via S. Sofia 64, 95127 Catania, Italy ⁶Centre for Quantum Technologies, National University of Singapore 117543, Singapore

October 30, 2023

Abstract

The coherent quantum transport of matter wave through a ring-shaped circuit attached to leads defines an iconic system in mesoscopic physics that has allowed both to explore fundamental questions in quantum science and to draw important avenues for conceiving devices of practical use.

Here we study the source-to-drain transport of excitations going through a ring-network, without propagation of matter waves. We model the circuit in terms of a spin system with specific long-range interactions that are relevant for quantum technology, such as Rydberg atoms trapped in optical tweezers or ion traps. Inspired by the logic of rf- and dc-SQUIDs, we consider rings with one and two local energy offsets, or detunings. As a combination of specific phase shifts in going though the localized detunings and as a result of coherent tunneling, we demonstrate how the transport of excitations can be controlled, with a distinctive dependence on the range of interactions.

1 Introduction

Quantum transport in mesoscopic circuits deals with matter propagating in networks characterized by a spatial scale comparable with the particles coherence length [1, 2]. In this regime, quantum effects as quantum tunneling, conductance quantization, flux-quantization, Aharanov-Bohm effect, etc, play a prominent role [3, 4, 5]. Recently, quantum transport of cold atoms guided in versatile and flexible laser-generated circuits has been studied both theoretically and experimentally [6, 7, 8, 9, 10]. Indeed, through widely tunable interactions and disorder, new schemes in mesoscopic physics have been defined, both for bosonic and fermionic sytems, with a great potential for basic quantum science and applications [11, 12].

In this paper, we refer to one of the most iconic systems of mesoscopic physics that has led to far reaching implications: a mesoscopic ring-shape track connected to source and drain leads [1, 2, 13, 14, 15]. The tunneling through scattering impurities or localized barriers placed in the ring circuit can induce specific phase shifts in the particles wave function [16]. In this way, the source-to-drain current can be controlled, a fact that is relevant both to study fundamental features of quantum interference and to engineer mesoscopic quantum devices with enhanced performances. With a similar logic, neutral bosonic matter wave current oscillations have been predicted and analysed in Ref. [10]. Rings with one or two localized barriers can define the bosonic analog of rf- and dc-SQUIDs[17, 18, 19, 12]. Such cold-atom implementations pave the way to rotation sensors based on the Sagnac effect [20].

Here, we study the source-to-drain quantum transport through a ring-shaped circuit in which, instead of matter, the dynamics occur in terms of excitations. The implementation we rely on is a circuit made of Rydberg atoms trapped in tweezers or ions trapped in suitable electromagnetic fields [21, 22, 23, 24]. Indeed, in such systems the motion of the atoms or of the ions can be neglected, with the relevant dynamics occurring as the transfer of excitations of internal energy states of the system. Moreover, both Rydberg atoms and ions can be trapped in a large variety of different geometries and with a remarkable control of the physical conditions [25, 26, 27, 28].

In contrast with the cases considered so far, here we deal with systems with a long-range interaction capturing the characteristic physics of Rydberg atoms and trapped ions [29, 30, 31].

We implement a specific quench dynamics that we demonstrate to lead to the sought drainto-source excitation transport: Initialized in the source, the excitation propagates along the two arms of the ring and, after many scattering events determined by the (long range) interaction, reaches the drain. Dealing with a closed system, the excitations population in the source and in the drain displays characteristic oscillations. We shall see that the entire excitation dynamics and then the source-to-drain transport can be controlled by suitable energy level detunings localized in the ring track. Such detunings play a similar role of what the aforementioned local potential barriers do for matterwave [10]. We shall see that the presence of detunings gives a non trivial time-dependent phase to the time-evolved state. Inspired by the rf-and dc-SQUID concept, we study the cases of one and two localized detunings.

The paper is organized as follows: in Sec. 2, we introduce the model and the possible experimental platforms on which it can be realized. In Sec. 3, we study the dynamics of the leads and the ring population in presence of a single detuning in one arm of the ring. In Sec. 4, we perform the same type of simulations but in presence of two detunings, one for each arm of the ring, with the same height and the same sign first, with opposite sign secondly. Our conclusions are drawn in Sec. 5. The Appendix provide a more detailed analysis of the model properties and of the mechanisms that lead to the peculiar dynamics observed in the main text.

2 Model and Methods

The system is comprised of two leads, the source (S) and the drain (D), each of them modeled by a single site containing at most one excitation, connected to a ring network (R) of N_r sites. Localized detunings are placed in the ring lattice and arranged in different configurations (see Fig.1). The excitation in each site is modelled as a two-level system $\{|\uparrow\rangle, |\downarrow\rangle\}$. The Hamiltonian of the system reads

$$\hat{\mathcal{H}} = \hat{\mathcal{H}}_{\mathcal{R}} + \sum_{\mathcal{L}=\mathcal{S},\mathcal{D}} \hat{\mathcal{H}}_{\mathcal{L}\mathcal{R}} + \hat{\mathcal{H}}_{\mathcal{S}\mathcal{D}},\tag{1}$$

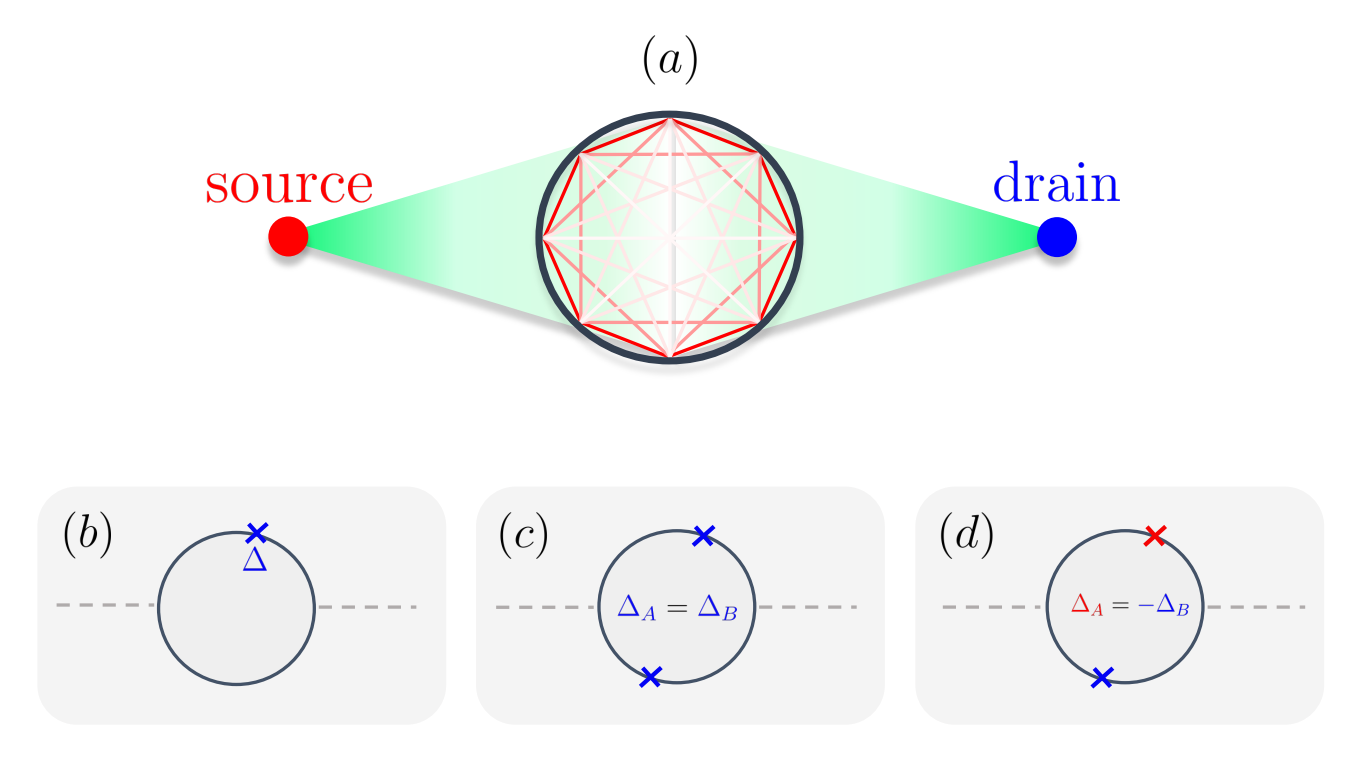


Figure 1: (a) Pictorial representation of the system: two sites, a source and a drain are connected to a ring. Sites are connected with hopping that scales as $1/d^{\alpha}$, d being the distance between sites. In the boxes three possible configurations of the ring: (b) One barrier, (c) two barriers with the same sign, (d) two barriers with opposite sign. The number of sites in the ring is such that $N_r/2$ is odd. The asymmetric location of the detunings with respect to the leads is chosen to have different paths for the excitation on the two arms.

with

$$\hat{\mathcal{H}}_{\mathcal{R}} = \sum_{i < j \in \mathcal{R}} \frac{g}{d_{ij}^{\alpha}} \left(\hat{\sigma}_i^+ \hat{\sigma}_j^- + \text{H.c.} \right) + \hat{\mathcal{H}}_{\text{Det}}, \tag{2a}$$

$$\hat{\mathcal{H}}_{\mathcal{L}\mathcal{R}} = \sum_{j \in \mathcal{R}} \frac{g}{d_{\mathcal{L},j}^{\alpha}} \left(\hat{\sigma}_{j}^{+} \hat{\sigma}_{\mathcal{L}}^{-} + \text{H.c.} \right), \quad (\mathcal{L} = \mathcal{S}, \mathcal{D}),$$
 (2b)

$$\hat{\mathcal{H}}_{\mathcal{S}\mathcal{D}} = \frac{g}{d_{\mathcal{S}\mathcal{D}}^{\alpha}} \left(\hat{\sigma}_{\mathcal{S}}^{+} \hat{\sigma}_{\mathcal{D}}^{-} + \text{H.c.} \right), \tag{2c}$$

$$\hat{\mathcal{H}}_{\text{Det}} = \sum_{j \in \mathcal{R}} \sum_{j_l \in \mathcal{I}} \Delta_j \hat{n}_j \delta_{j, j_l}.$$
 (2d)

Here $\hat{\sigma}_j^{\alpha}$ ($\alpha=x,y,z$) denote the spin-1/2 Pauli matrices on the jth atom and $\hat{\sigma}_j^{\pm}=\frac{1}{2}(\hat{\sigma}_j^x\pm i\hat{\sigma}_j^y)$ are the corresponding raising/lowering operators, such that $\hat{\sigma}_j^+|\downarrow_j\rangle=|\uparrow_j\rangle$ and $\hat{\sigma}_j^-|\uparrow_j\rangle=|\downarrow_j\rangle$. The Hamiltonian part (2a) describes the intra-ring hopping in the presence of detunings (2d), while Eq. (2b) describes the leads-ring hopping and Eq. (2c) describes the direct source-drain hopping. We suppose that the excitation $|\uparrow\rangle$ can hop from site to site with a strength scaling as $1/d^{\alpha}$, with d denoting the distance between the sites and α a parameter inversely related to the hopping range. In particular, d_{ij} is the intra-ring distance, $d_{\mathcal{S},j}$ and $d_{\mathcal{D},j}$ are the distances between the leads and all the sites of the ring, while $d_{\mathcal{S}\mathcal{D}}$ is the distance between source and drain (see A). We work in the weak leads-ring coupling limit, corresponding to $K_{nn} \ll J_{nn}$, where K_{nn} and J_{nn} are the leads-ring and intra-ring nearest-neighbor hopping strengths, respectively (see A for details). Finally, we fix the total number of atoms in such a way that $N_r/2$ is odd. In this paper, we consider $1 \leq \alpha \leq 3$, with the nearest-neighbor and the fully connected models corresponding to $\alpha \to \infty$ and $\alpha = 0$, respectively. Trapped ions in linear chains provide a

powerful platform to realize quantum spin Hamiltonians in which the spin-spin interaction or the hopping strength scale approximatively as $d^{-\alpha}$, where $\alpha \in (0,3)$ [21, 32, 33, 29, 34]; the $|\downarrow\rangle$ and $|\uparrow\rangle$ states are two internal electronic states of the ions. The implementation of different geometries is more challenging, but two-dimensional spin Hamiltonians have been realized as well [36, 37, 38, 34, 39, 40]. Concerning rings, circular traps of ions have been realized as well [27, 41, 42].

The case $\alpha=3$ can be also implemented in Rydberg atoms. For such systems, $|\downarrow\rangle$ and $|\uparrow\rangle$ are two Rydberg states of opposite parity (i.e., $|S\rangle$ and $|P\rangle$) [23, 30, 43, 44]. Thanks to the high control on the geometry in which the atoms are located in these systems [25, 26], it is possible to realize ring-shaped and more complicated geometries [45]. We consider three possible configurations of the localized detunings in the ring lattice. The case $\mathcal{I}=\{j_0\}$ corresponds to one localized detuning (see Fig. 1b), the path crossed by the excitation in the two arms of the ring is clearly different; the two other cases correspond to $\mathcal{I}=\{j_A,j_B\}$ with j_A and j_B in diametrical position, $\Delta_A=\Delta_B$ and $\Delta_A=-\Delta_B$ respectively (see Fig. 1c,d). Since the distances $d_{\mathcal{S},j_A}\neq d_{\mathcal{S},j_B}$, we observe that, also in this case, the path crossed by the excitation fraction in one arm of the ring is different from the other. The local detunings are experimentally feasible through local AC-Stark shifts with a focused laser on the site of interest.

To initialize the transport, we apply a specific quench protocol. At t=0 we localize a single excitation in the source:

$$|\psi(0)\rangle = |\uparrow\rangle_{\mathcal{S}} \otimes |\downarrow, ..., \downarrow\rangle_{\mathcal{R}} \otimes |\downarrow\rangle_{\mathcal{D}}, \tag{3}$$

then we evolve the system via Schrödinger equation $|\psi(t)\rangle = \exp(-i\hat{\mathcal{H}}t) |\psi(0)\rangle$. To monitor the dynamics, we scrutinize the number of excitations in the source, the ring, and the drain:

$$\hat{n}_{\mathcal{S}} = \frac{1}{2}(\hat{1}_{\mathcal{S}} + \hat{\sigma}_{\mathcal{S}}^z), \quad \hat{n}_{\mathcal{R}} = \frac{1}{2} \sum_{j \in \mathcal{R}} (\hat{1}_j + \hat{\sigma}_j^z), \quad \hat{n}_{\mathcal{D}} = \frac{1}{2}(\hat{1}_{\mathcal{D}} + \hat{\sigma}_{\mathcal{D}}^z). \tag{4}$$

We comment that, since the Hamiltonian conserves the total number of excitations $\hat{n}_{tot} = \hat{n}_{\mathcal{S}} + \hat{n}_{\mathcal{R}} + \hat{n}_{\mathcal{D}}$, with the initial condition (3), we can work in the one-excitation sector, namely $\langle \psi(t)|\hat{n}_{tot}|\psi(t)\rangle = 1$. Thus, we define the projector \hat{P} represented by a $N \times 2^N$ matrix that projects operators and states of the full Hilbert space into operators and states of the one excitation sector. The states and operators with which we will work are of the form $\hat{P}|\psi\rangle$ and $\hat{P}\hat{O}\hat{P}^{\dagger}$, $|\psi\rangle$ and \hat{O} being a generic state and operator acting on the full Hilbert space.

3 Dynamics in the presence of a single detuning

We first study the dynamics of the number of excitations in the system, in the presence of a single localized detuning (2d) (see Fig.1b). The results are summarized in Fig. 2, reporting the population dynamics $P_j = \langle \hat{n}_j \rangle$ in the source, the ring and the drain. Then, we analyze the phase difference behavior between the two arms of the ring. In particular, the phase difference between two opposite sites located in the two different arms.

3.1 Excitation dynamics in presence of a single detuning

Because of the weak coupling assumption, insights on the general features of the excitations dynamics can be achieved by looking at the energy (discrete) spectrum of the leads and ring separately. The initial state will be denoted as $|\psi(0)\rangle = |\mathcal{S}\rangle$, assumed at zero energy. The ring Hamiltonian in the single particle sector has N_r eigenstates with non-zero energies; they result to be doubly degenerate except the ground and highest excited states. The role of the localized detuning is to break the degeneracies and shift the ring levels. For specific values of

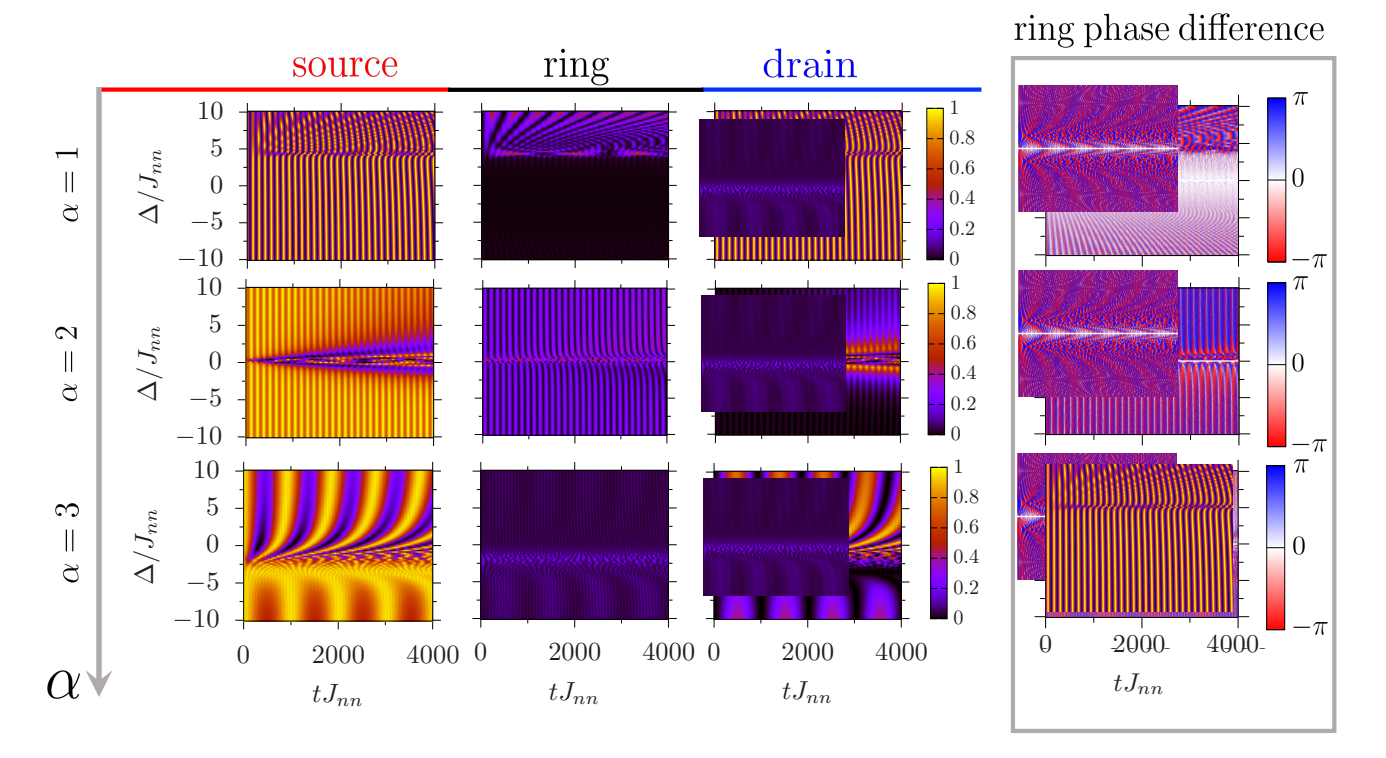


Figure 2: Panels on center-left: excitation populations in the source $P_{\mathcal{S}}$, in the ring $P_{\mathcal{R}}$ and in the drain $P_{\mathcal{D}}$ for three different values of the hopping range $\alpha=1,2,3$ from top to bottom. Three panels on the right: ring phase difference $\delta\phi$ between two opposite sites located in the two arms of the ring for the three values of α considered. Excitation populations and phase difference are plotted in function of time (x-axis) and detuning (y-axis) of the single barrier located in the ring at position $j_0 = \lceil N_r/4 \rceil$. The population values are indicated by the color bar that goes from 0 to 1, the phase difference by the one that goes from $-\pi$ to π . The number of sites in the ring is $N_r = 14$. The leads-ring coupling is $K_{nn} = J_{nn}/10$.

the detuning Δ_{res} the ring energy levels can be resonant with the initial source state $|\mathcal{S}\rangle$ (see B). In this case, the excitation is transferred from source to the drain and backward to the source, through the ring that is well populated, see Fig. 2. Since the total number of excitations is conserved and the ring is populated, during its time evolution the population is distributed along leads and channel. Far from resonance, coherent source-drain oscillations display a marked dependence on Δ as soon as α increases. This means that the source-drain dynamics depends on the characteristics of the ring and not only on the source-drain direct coupling $\hat{\mathcal{H}}_{\mathcal{SD}}$. In this regime, the transport can occur in terms of cotunneling processes [4, 46, 47]: Similarly to the transport occurring in quantum dots in the regime in which sequential tunneling cannot happen (because of the Coulomb blockade), a source-to-drain transport in our system can occur through virtual transitions in the ring energy levels; in this regime, the ring is found with a low population of excitations.

Due to the long-range nature of the interaction we consider in the present paper, specific features of the system emerge when leads and ring-shape track are not treated separately (see Fig. 1). Specifically, because of a combination of geometrical effects and energy level configuration, we found that the transport displays a marked dependence on α , especially in the (leads-ring) nearly resonant regimes. For $\alpha = 1$, the source and drain populations oscillate regularly until $\Delta/J_{nn} \approx 5$, value for which the rings starts to be populated and the dynamics inside the leads is less regular. Far from that value, the ring is not populated and the source-drain oscillations does not depend on the detuning. For $\alpha = 2$, the dynamics is quite different: in the (Δ,t) plane appears a V-pattern. On the borders of the V, the drain and source populations

are respectively maximum and minimum. The vertex of the V is in correspondence of Δ_{res} , where the ring is more populated. Another important feature of this regime is the population dynamics for values of detuning far from the resonance. The source is at every time the most populated, the drain the less populated. The ring population is small but not zero, it shows a weak oscillation with those of the source.

The $\alpha=3$ regime is characterized by slow (compared with the previous cases $\alpha=1$ and $\alpha=2$) coherent transfer of excitation from the source to the drain interrupted at the value of Δ for which source and ring are resonant. As a specific feature of this case, we note a localization of the excitation in the source occurring for values of Δ slightly smaller of Δ_{res} . Indeed, such localized source state appears in the analysis of the full leads-ring system Hamiltonian spectrum (see D). For different values of Δ the complete states have also substantial projection in the drain state and therefore the dynamics results to display the characteristic source-drain coherent oscillations.

3.2 Phase difference dynamics in presence of a single detuning

We now analyse the phase of the excitations flow between the two arms of the ring. To this end, we compute the phase difference between two symmetric sites of the arms, being $i = N_r/2 - 1$ and $j = N_r/2 + 1$. The argument of the two-body correlator $\langle \hat{\sigma}_i^+ \hat{\sigma}_j^- \rangle$ gives the phase difference $\delta \phi$ between the two sites, details are reported in E. With the sake of corroborating our results analytically, we analysed a straight finite chain. Indeed, we found that the phases of the coefficients of the time evolved state in the position basis depend non trivially on Δ .

Fig. 2 reports the phase difference in function of time and detuning for different values of α . Our results indicate that, as a localized potential barrier does for matter waves, the localized detuning causes a phase shift between the two arms of the ring. The dependence of the phase difference on the detuning is evident for each value of α . In particular, it follows the ring population oscillation frequency. However, also when the ring population oscillation amplitude is small and hardly observable, the phase difference can present non negligible oscillations. For instance, for $\alpha=1$ and negative values of the detuning, there are evident phase difference oscillations while the ring is basically not populated. In a window around $\Delta=0$, the phase difference is zero because the paths on the two arms are the same. On the other hand, in correspondence of the resonances, as soon as the ring becomes populated, we observe strong oscillations in the phase difference.

In general, the phase oscillation follows the population oscillation, independently on the amplitude of the latter. If there is a little amount of excitation that moves in the ring, the phase difference oscillates with an amplitude that is significantly different from zero. For instance, for $\alpha = 1$ and negative detuning, we observe phase oscillations also if the ring population is very small.

4 Dynamics in presence of double detuning

In this section we study the source-to-drain dynamics of number of excitations in the case in which two atoms in the ring are detuned - see Sec. 2. We first study the case in which the two detunings have the same sign and then the case in which they have same magnitude but opposite sign.

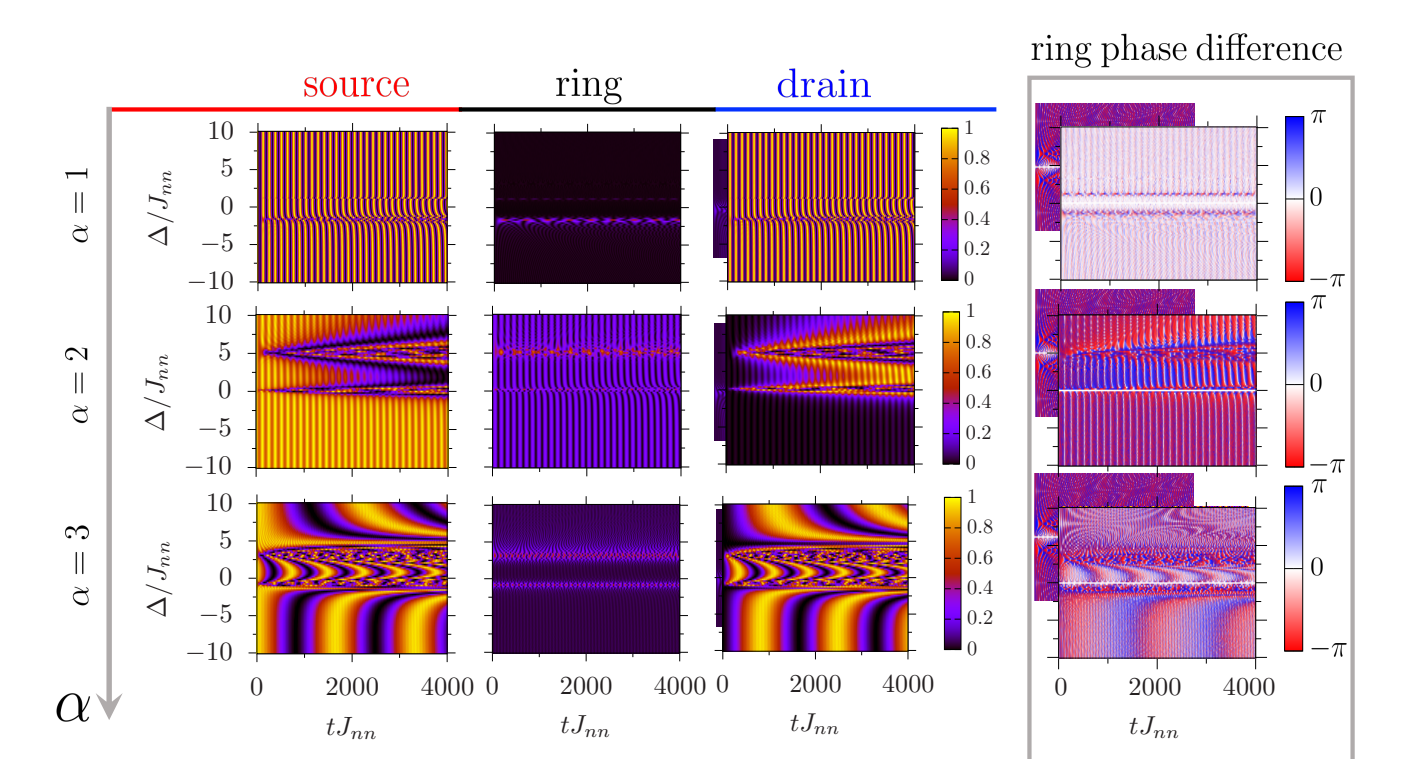


Figure 3: Populations and ring phase difference as in Fig.2 for two detunings located at $j_A = \lceil N_r/4 \rceil$ and $j_B = \lceil 3N_r/4 \rceil$, the detunings are equal: $\Delta_A = \Delta_B = \Delta$. The Hamiltonian parameters are set as in Fig.2.

4.1 Excitation dynamics in presence of double detunings with the same sign

Also in this case, the hopping range has pronounced effects on the dynamics. The combined energy shifts caused by the two detunings and hopping range give rise to a resonant transport occurring in correspondence to two resonances (instead of the one in the previous single detuning case) that turns out to be not symmetric with respect to $\Delta=0$. The nature of the level shift that brings to resonance can be accessed analytically and numerically looking at the ring spectrum respectively in the nearest neighbor and long range cases (see B). Fig. 3 reports the population dynamics.

For $\alpha=1$, the dynamics is characterized by fast oscillations between source and drain with a frequency that is nearly independent of detuning. The ring is almost never populated except for the two Δ_{res} values, where the dynamics in the leads result to be erratic. In the case $\alpha=2$, the dynamics clearly changes. Far from resonances, the dynamics result to be similar to the one observed in the single detuning case. In this case we see two V-shaped patterns in the (Δ,t) plane around the two resonances. We notice a depletion in the source and a filling of the drain in correspondence of the meeting points of the two V-shaped patterns. Finally, as in the case with single detuning, for $\alpha=3$ the transport between source and drain is slower and more affected by the process occurring in the ring track. In particular, tuning Δ the transport in the system shows markedly different features. For large (positive or negative) values of Δ , the transport of excitations is slow-down, with the ring resulting weakly populated. Around the two resonant levels the transport becomes erratic and the ring results populated. In between the two resonances, we observe regular and fast oscillations of the population in the leads.

4.2 Excitation dynamics in presence of double detunings with opposite sign

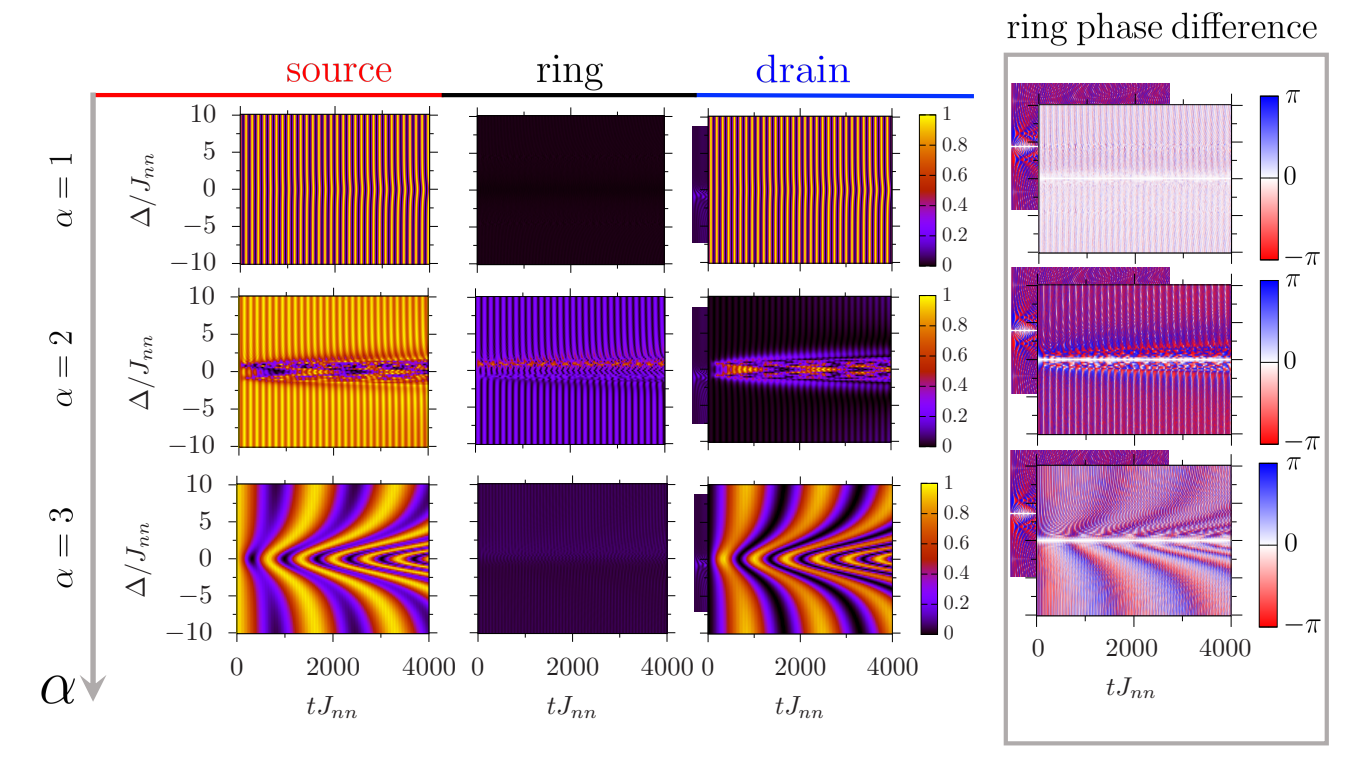


Figure 4: Populations and ring phase difference as in Fig.2 for two detunings located at $j_A = \lceil N_r/4 \rceil$ and $j_B = \lceil 3N_r/4 \rceil$, the detunings have equal magnitude but opposite sign: $\Delta_A = -\Delta_B = \Delta$. The Hamiltonian parameters are set as in Fig.2.

We complete our analysis by the study of the configuration of double equal barrier with opposite sign. Also here, the three different values of α denote three different regimes. The double barrier regime is basically different from the other two because the first perturbative order energy correction is zero - see B. Thus, it is harder to get resonances.

For $\alpha=1$, the dynamics is characterized by fast oscillations between source and drain, the ring is never resonant with initial state and so is never populated. For $\alpha=2$, the ring spectrum presents two symmetric resonances (instead of the asymmetric ones of the previous subsection) with the zero energy mode. This feature is corroborated by a perturbative analysis showing that the resonances depends as Δ^2 (see B). For large (positive and negative) values of Δ , the population in the drain is minimal, while a small fraction of excitation oscillates between source and ring. For values of Δ between the two resonances, a source-drain slow oscillation given by the recombination of the two V-shaped patterns appear. The regime corresponding to $\alpha=3$ is characterized by slow coherent oscillations between the two leads, the ring track being weakly populated. Differently from the $\alpha=1$ case, the value of Δ determines the oscillation frequency between source and drain. It is found that the excitation transfer slows down by increasing Δ .

4.3 Two arms phase difference with double detuning

Figures 3 and 4 report the phase difference between the sites of the two arms closest to the drain in presence of two detunings. As in the case of single detuning, the phase difference oscillations are minima in amplitude for $\alpha = 1$ far from resonances. For $\alpha = 2$ we observe strong phase difference oscillations, evident oscillations are observed also for $\alpha = 3$. In all the cases analyzed so far, the

phase difference oscillations follow in frequency those of populations. Also in this case, the phase oscillations are correlated to the ring population oscillations: the phase oscillation amplitude is bigger when the ring is more populated. However, a little amount of excitation in the ring is sufficient to have substantial oscillations in the phase.

In E we also study the phase difference dynamics for different locations of the detunings. As expected, the phase oscillations strongly depend on it; if the detunings are located in such a way that the excitation fractions follow the same paths on the two arms of the ring, the phase difference is zero for any Δ . This result can be achieved putting two equal detunings in two diametrically opposite zones of the arms. Otherwise, if the resonance location in Δ is the same and the two paths are different, the dynamics differs with the one considered here with specific features depending on the geometry.

5 Discussions

We discussed the source-drain excitation transport through a ring lattice track in which in one or two sites the atoms are detuned by Δ respect to the others; such detunings act as local energy shifts in the system and therefore they play the role of localized impurities. Motivated by the know-how in quantum technology, the system is described by long range XY Hamiltonian with $1/d^{\alpha}$ interaction; specific values of α that are relevant for ion traps [22, 32, 48] and Rydberg atoms [23] localized in optical tweezers are considered. This feature should be contrasted with previous studies corresponding to nearest-neighbor hopping [10]. As we detailed below, the transport can be controlled by tuning Δ , with distinctive features of α .

The energy excitation is initialized in the source lead, with a zero energy state. Then the excitation is transferred to the ring by quenching the interaction with the rest of the system. In the weak leads-ring tunneling regime, we note that, once the excitations are transferred to the ring track, they propagate within the ring with a fast time dynamics. The presence of localized detunings causes the shift of the energy levels of the XY Hamiltonian of the ring and, for specific values of Δ , a state resonant with the source one can occur. Inspired by rf- and dc-SQUIDs, we considered the two cases of one and two detunings; in turn, we considered two detunings with the same sign or with opposite sign.

Resonant and non-resonant transport display distinctive features. For resonant transport, the excitation can be transferred from the source to drain, while the ring track is moderately occupied. Far from resonance, the excitation oscillates between source and drain, minimmally populating of the ring on the the observed time scales. The nature of the oscillation depends on the characteristics of the ring.

Clearly, we observe that, the far-off-resonance dynamics is nearly independent on the detuning (indicating that the detuned sites are bypassed by the long range hopping). By increasing α , we observe a non trivial effect of detunings which is first localized around the resonant transport and then extended to the non-resonant dynamics.

By studying the phase difference between upper and lower arms of the ring, we can conclude that the detuning can affect the phase of excitations (similarly to the effect of barriers in matterwave propagation). The corresponding phase difference is observed to oscillate, even for small population oscillations. Phase difference and population oscillation frequencies are related.

Besides its own interest, we think our work is relevant to conceive devices of practical value employing Rydberg atoms or trapped ions. Finally, we point out that our logic can be feasibly extended to systems with different geometries, also in presence of noise.

Acknowledgments

We thank Giampiero Marchegiani and Tobias Haug for useful discussions. The Julian Schwinger Foundation grant JSF-18-12-0011 is acknowledged. The Julian Schwinger Foundation grant JSF-18-12-0011 is acknowledged. OM also acknowledges support by the H2020 ITN "MOQS" (grant agreement number 955479) and MUR (Ministero dell'Università e della Ricerca) through the PNRR MUR project PE0000023-NQSTI. Numerical computations have been performed using the Julia packages QuantumOptics.jl [49].

Appendix A Distance and weak coupling limit

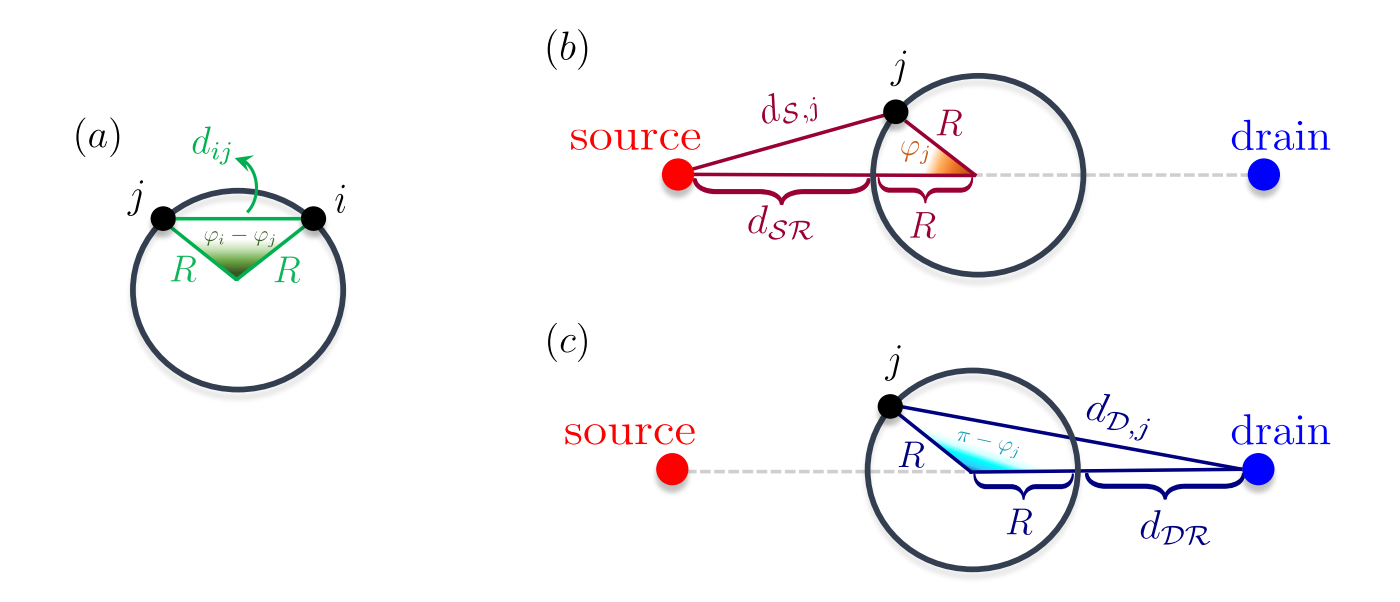


Figure 5: Pictorial representation of distances in the system considered. Panel (a): intra-ring distance between two sites located at positions i and j. Panel (b): source-ring distance. Panel (c): drain-ring distance.

Here we provide a proper definition of the intra-ring and ring-leads distances, then we specify what we mean for weak ring-leads coupling. To define the distances, we first need to introduce an appropriate labeling of the atoms in the ring. Thus, supposing to work with an even number of sites in the ring, we label as N_r the site closest to the source and $N_r/2$ the site closest to the drain. We identify with $\varphi_j = 2\pi j/N_r$ the angle associated to the site j of the ring. Given this labeling, we can write the source-ring distance as

$$d_{\mathcal{S},j} = \sqrt{(d_{\mathcal{SR}} + R)^2 + R^2 - 2(d_{\mathcal{SR}} + R)R\cos\varphi_j}$$
 (5)

where d_{SR} is the smallest distance between source and ring, precisely, it is the distance between the source and the site N_r ; R is the radius of the ring. At the same time, the drain-ring distance is

$$d_{\mathcal{D},j} = \sqrt{(d_{\mathcal{DR}} + R)^2 + R^2 - 2(d_{\mathcal{DR}} + R)R\cos(\pi - \varphi_j)}$$
 (6)

where $d_{\mathcal{DR}}$ is the smallest distance between source and ring, that is the distance between drain and site $N_r/2$. The intra-ring distance is

$$d_{ij} = 2R \sin\left(\frac{|\varphi_i - \varphi_j|}{2}\right) = 2R \sin\left(\frac{\pi|i - j|}{N_r}\right). \tag{7}$$

Finally, we introduce the source-drain distance. Given $d_{\mathcal{DR}}$, $d_{\mathcal{SR}}$ and the radius of the ring, the aforementioned distance is $d_{\mathcal{SD}} = d_{\mathcal{SR}} + 2R + d_{\mathcal{DR}}$. A pictorial representation of the distances is reported in Fig.5. Given a proper definition of the intra-ring and leads-ring distances, we can introduce the intra-ring nearest neighbor hopping

$$J_{nn} = \frac{g}{d_{nn}^{\alpha}}, \qquad d_{nn} = 2R \sin\left(\frac{\pi}{N_r}\right) \tag{8}$$

and the leads-ring nearest neighbor hopping

$$K_{nn} = \frac{g}{d_{\mathcal{SR}}^{\alpha}} = \frac{g}{d_{\mathcal{DR}}^{\alpha}},\tag{9}$$

where we are supposing that $d_{SR} = d_{DR}$. In the main text we work in the weak leads-ring coupling limit $K_{nn} \ll J_{nn}$, which means $d_{SR}^{\alpha} \gg d_{nn}^{\alpha}$. Thus, if we consider $K_{nn} = J_{nn}/M$, M being an integer bigger than one, the distances will be related by $d_{SR} = M^{1/\alpha} d_{nn}$.

Appendix B Ring spectral analysis

In the weak coupling regime, the ring and leads modes can be treated separately, their relation is crucial to understand the nature of the transport. The initial state of our protocol is a zero energy state, thus, the presence of zero energy modes in the ring is responsible for the population of the latter during the dynamics. In absence of zero energy modes in the ring, the latter will not be populated and the dynamics will result in coherent oscillations between source and drain. In this section, we will study the effect of localized detunings on the spectrum of an XY model in a ring. We will first use a perturbative approach to study the effect of the detunings on the spectrum of the nearest neighbor model; it is instructive to understand the possible presence of resonances between ring and drain. Then, we will numerically analyze the modification of the ring Hamiltonian spectrum due to the long range hopping paying particular attention to the changes in terms of resonances with zero energy modes. We will work in the one excitation sector of the Hamiltonian.

B.1 Nearest neighbor XY energy shift due to detuning

Let us consider the generic Hamiltonian

$$\hat{\mathcal{H}} = \hat{\mathcal{H}}_0 + \lambda \hat{\mathcal{H}}'. \tag{10}$$

 $\hat{\mathcal{H}}_0$ is the unperturbed Hamiltonian, while $\hat{\mathcal{H}}'$ is the perturbation Hamiltonian whose intensity λ is supposed to be small with respect to the unperturbed eigenvalues. We consider an that Hamiltonian possesses at least a couple of degenerate states $|E_a^0\rangle$ and $|E_b^0\rangle$ such that

$$\hat{\mathcal{H}}_0 | E_{a,b}^0 \rangle = E^{(0)} | E_{a,b}^0 \rangle \,.$$
 (11)

From now on we will work in the subspace spanned by these two states. Let us introduce the matrix element

$$W_{ij} = \langle E_i^0 | \hat{\mathcal{H}}' | E_j^0 \rangle. \tag{12}$$

The first order correction to the unperturbed eigenvalue is [50]

$$E_{\pm}^{(1)} = \frac{W_{aa} + W_{bb} \pm \sqrt{(W_{aa} - W_{bb})^2 + 4|W_{ab}|^2}}{2}, \quad E = E^{(0)} + \lambda E_{\pm}^{(1)}. \tag{13}$$

Now, we consider a XY model on a ring composed of N_r sites perturbed by a localized detuning term:

$$\hat{\mathcal{H}} = J \sum_{j=1}^{N_r} \left(\hat{\sigma}_j^+ \hat{\sigma}_{j+1}^- + \text{H. c.} \right) + \Delta \sum_{j=1}^{N_r} \hat{n}_j \delta_{j,j_0} = \hat{\mathcal{H}}_0 + \Delta \hat{\mathcal{H}}'$$
 (14)

where here Δ is the perturbative parameter and we work in the one excitation sector. The unperturbed Hamiltonian can be diagonalized transforming the spins in fermions via Jordan Wigner transformation [51, 52]. The basic idea of the Jordan wigner transformation is to transform the spin Hamiltonian into a fermionic Hamiltonian. To do that, we introduce the JW fermions

$$\hat{c}_j = \left(\prod_{\ell < j} \hat{\sigma}_\ell^z\right) \hat{\sigma}_j^-, \quad \hat{c}_j^{\dagger} = \left(\prod_{\ell < j} \hat{\sigma}_\ell^z\right) \hat{\sigma}_j^+; \tag{15}$$

the resulting unperturbed model is a fermionic non-diagonal Hamiltonian. In the one excitation sector, the fermionic operators are rotated through the transformation

$$\hat{c}_{j}^{\dagger} = \frac{1}{\sqrt{N_r}} \sum_{n=1}^{N_r} e^{2\pi i j n/N_r} \hat{d}_{n}^{\dagger} \tag{16}$$

and the diagonal unperturbed Hamiltonian is obtained

$$\hat{\mathcal{H}}_0 = \sum_{n=1}^{N_r} E_n^{(0)} \hat{d}_n^{\dagger} \hat{d}_n, \quad E_n^{(0)} = 2J \cos\left(\frac{2\pi n}{N_r}\right). \tag{17}$$

We define the momentum $k=2\pi n/N_r$ and we can observe that the eigenvalues of the Hamiltonian are all doubly degenerate, except the ground and the maximum energy states. We can easily observe that the couples of degenerate eigenstates are of the form $|k\rangle$ and $|2\pi - k\rangle$ (or alternatively $|n\rangle$ and $|N_r - n\rangle$) which refers to states with momenta k and $2\pi - k$; thus, we can restrict our analysis in the subspace spanned by these two states. Here, the perturbation matrix element is

$$W_{k,k'} = \langle k | \hat{n}_{j_0} | k' \rangle. \tag{18}$$

To perform the computation it is convenient to transform the number operator in terms of Jordan Wigner fermions in the momentum space. Done that, the first matrix element to which we are interested is

$$W_{k,k} = \frac{1}{N_r} \sum_{m,m'=1}^{N_r} e^{-2\pi i m j_0/N_r} e^{2\pi i m' j_0/N_r} \langle n | \hat{d}_m^{\dagger} \hat{d}_{m'} | n \rangle$$

$$= \frac{1}{N_r} \sum_{m,m'=1}^{N_r} e^{2\pi i (m'-m)j_0/N_r} \delta_{n,m} \delta_{m',n} = \frac{1}{N_r} = W_{2\pi-k,2\pi-k}.$$
(19)

At the same time, the off-diagonal term will be

$$W_{k,2\pi-k} = \frac{1}{N_r} \sum_{m \, m'=1}^{N_r} e^{2\pi i (m'-m)j_0/N_r} \delta_{n,m} \delta_{m',N_r-n} = \frac{e^{2ikj_0}}{N_r} = W_{2\pi-k,k}^*.$$
(20)

Given the perturbation matrix elements, we can compute the first order energy corrections using eq.(13)

$$E_{\pm} = E^{(0)} + \Delta \frac{2 \pm 2}{2N_{\pi}}.\tag{21}$$

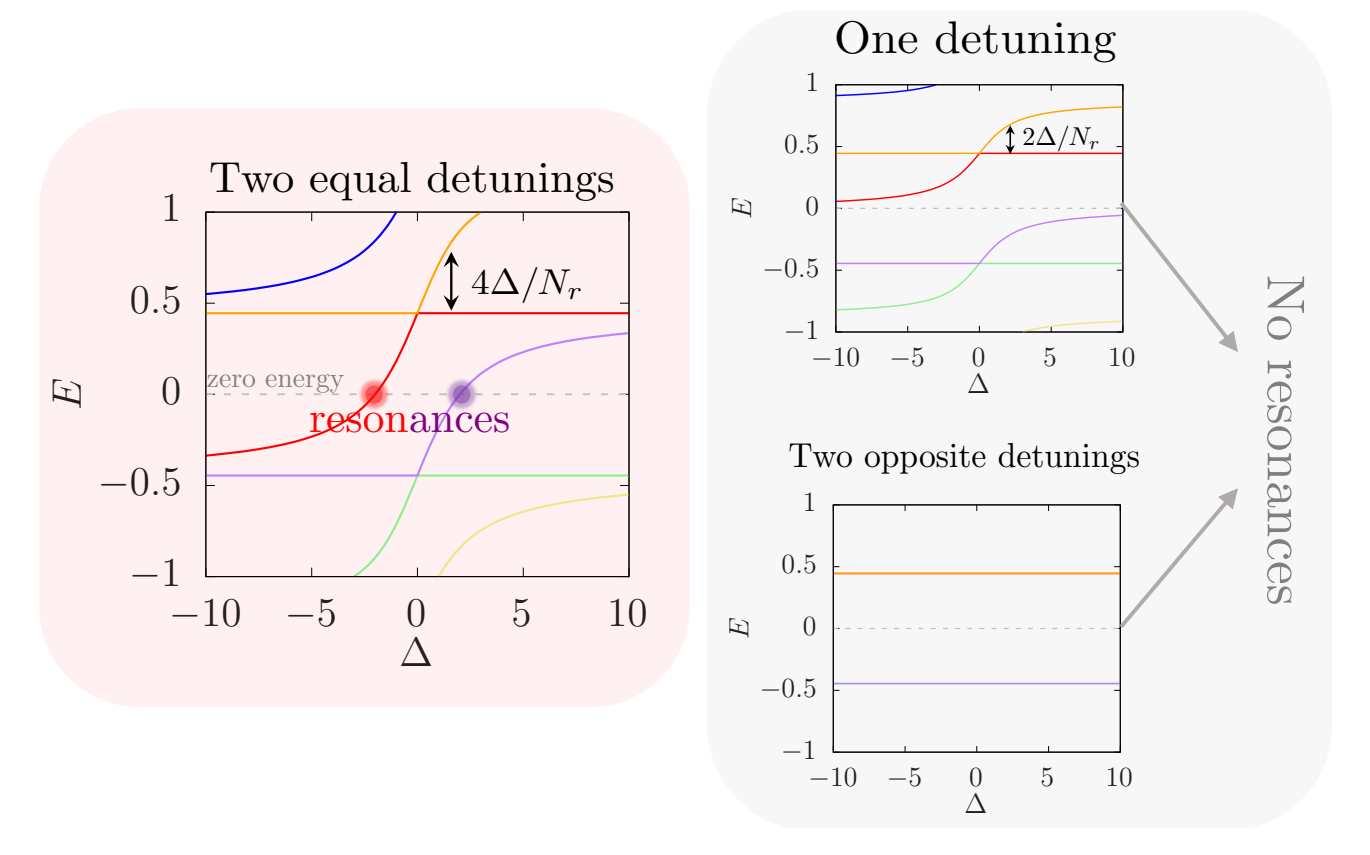


Figure 6: Numerical results for the spectrum of the nearest neighbor XY model in presence of localized barriers. Only energies with energy near to zero are reported. The number of sites is $N_r = 14$ and J = 1.

Thus, one of the two degenerate states remains unchanged and the other one is shifted by a factor $2\Delta/N_r$. The non degenerate eigenvalues E_{GS} and E_{max} are shifted by a common factor $W_{k_{GS},k_{GS}} = \langle k_{GS} | \hat{n}_{j_0} | k_{GS} \rangle = W_{k_{max},k_{max}} = \langle k_{max} | \hat{n}_{j_0} | k_{max} \rangle = \Delta/N_r$, where k_{GS} and k_{max} are the momenta associated respectively to the ground and the maximum energy state.

In the case of two detunings with the same sign, we have to consider the perturbation Hamiltonian

$$\hat{\mathcal{H}}' = \hat{n}_{j_A} + \hat{n}_{j_B}; \tag{22}$$

the perturbation matrix elements are

$$W_{k,k} = \frac{2}{N_r} = W_{2\pi - k, 2\pi - k},\tag{23}$$

$$W_{k,2\pi-k} = \frac{1}{N_r} \left(e^{2ikj_A} + e^{2ikj_B} \right) = W_{2\pi-k,k}^*. \tag{24}$$

Given the matrix elements, we can compute the energy correction for degenerate states via (13)

$$E_{\pm} = E^{(0)} + \Delta \frac{2 \pm \sqrt{2(1 + \cos(2k(j_A - j_B)))}}{N_r}.$$
 (25)

If we set the barriers in opposite sides of the ring, i.e. $j_A = \lceil N_r/4 \rceil$ and $j_B = \lceil 3N_r/4 \rceil$, in such a way that $|j_A - j_B| = N_r/2$, we obtain a shift of a factor 0 or $4\Delta/N_r$ for each state. On the other hand, the ground and the maximum energy state are both shifted by a factor $2\Delta/N_r$.

Finally, it is straightforward to observe that the first order correction to the energy states in presence of two barriers with opposite sign gives zero contribution at the first perturbative

order. To do that, it is sufficient to perform the same calculation done for two equal detunings with $\hat{\mathcal{H}}' = \hat{n}_{j_A} - \hat{n}_{j_B}$. If $|j_A - j_B| = N_r/2$, the first order energy correction is zero for each state of the spectrum.

Figure 6 reports the numerical results for the energy shifts in presence of localized detunings. Through the numerical computation we easily understand what happens beyond the first perturbative order. In particular, both for single and double equal detunings, the first order shifts in Δ are corrected for big values of the latter tending to flatten. The main difference between the two cases is the slope of the shift at small values of the detuning. The one of the single barrier case is smaller than the one of the double barrier case. Thus, while in the latter it is sufficient to permit to two levels to cross the zero energy mode, in the single barrier case the linear shift it is not sufficient. It is important to observe that we do not observe resonances in this case in our Δ range, it is possible that they are present for bigger values of the detuning. However, in the case of two opposite detunings, the degenerate states reported are not shifted even for more than first order contributions; then, we do not expect resonances, the dynamics is characterized by coherent oscillations between source and drain.

B.2 Long range XY energy shift due to detuning

For a nearest-neighbor XY model, the spectrum is symmetric with respect to the zero energy states, meaning that the energies are organized in pairs $\pm E_n$. We also showed how from the energy shifts we expect that the resonances are symmetric for $\Delta \to -\Delta$. However, the dynamics reported in the main text shows that for long range hopping this is not true. The ring population does not follow a symmetric behavior with respect to $\Delta = 0$. Therefore, a detailed analysis of the energy shift in the spectrum is important to understand the asymmetry in the dynamics. The model with which we work here is (2a).

Figure 7 reports the energy spectrum in all the three paradigmatic detuning configurations considered so far. Before analyzing the effect of the detuning, it is necessary to pay attention on the role of the inverse hopping range α for $\Delta=0$. We can immediately observe that for each value of α the degeneracies persist; on the other hand, a substancial shift of the levels is observed. Passing from $\alpha=5$ to $\alpha=1$ the levels lose their symmetry with respect to E=0 and tend to crush to a negative energy value. This means that the first E>0 and the first E<0 states does not possess anymore symmetric energy with respect to zero. When the detuning is switched on, the energy levels are shifted and cross the zero energy mode, the crossing is not symmetric in Δ simply because the starting energy levels from which the shift starts are anymore symmetric with respect to E=0.

To be more quantitative, let us first consider the case of the single barrier reported in Fig. 7(a). Here, the levels that cause resonances are the orange and red. Increasing the hopping range, the red and the orange levels are shifted downwards; during the shift, one of the two levels crosses the zero energy mode giving rise to one resonance at negative Δ . The purple level in the nearest neighbors limit is not sufficiently shifted to give rise to a positive resonance at positive Δ in the interval considered so far. Then, for one detuning, we have only one value or narrow range of Δ for which the ring becomes populated during the dynamics.

Figure 7(b) reports the results for two equal detunings: for each value of α there are at least two values of Δ for which the zero energy mode is crossed for the same reason for which it happens in the nearest neighbor XY model, meaning a bigger slope of the energy shift curve. In the two opposite detuning case reported in Fig. 7(c), the long range hopping is responsible for a shift of the energy levels that is quadratic in the detuning Δ . As in the nearest neighbor limit, also in presence of long range the first order correction is zero, thus the shift scales as Δ^2 with a coefficient that increases as α decreases. For this reason, it is possible to have symmetric resonances with respect to $\Delta = 0$. In particular, in the plots reported, resonances appear at

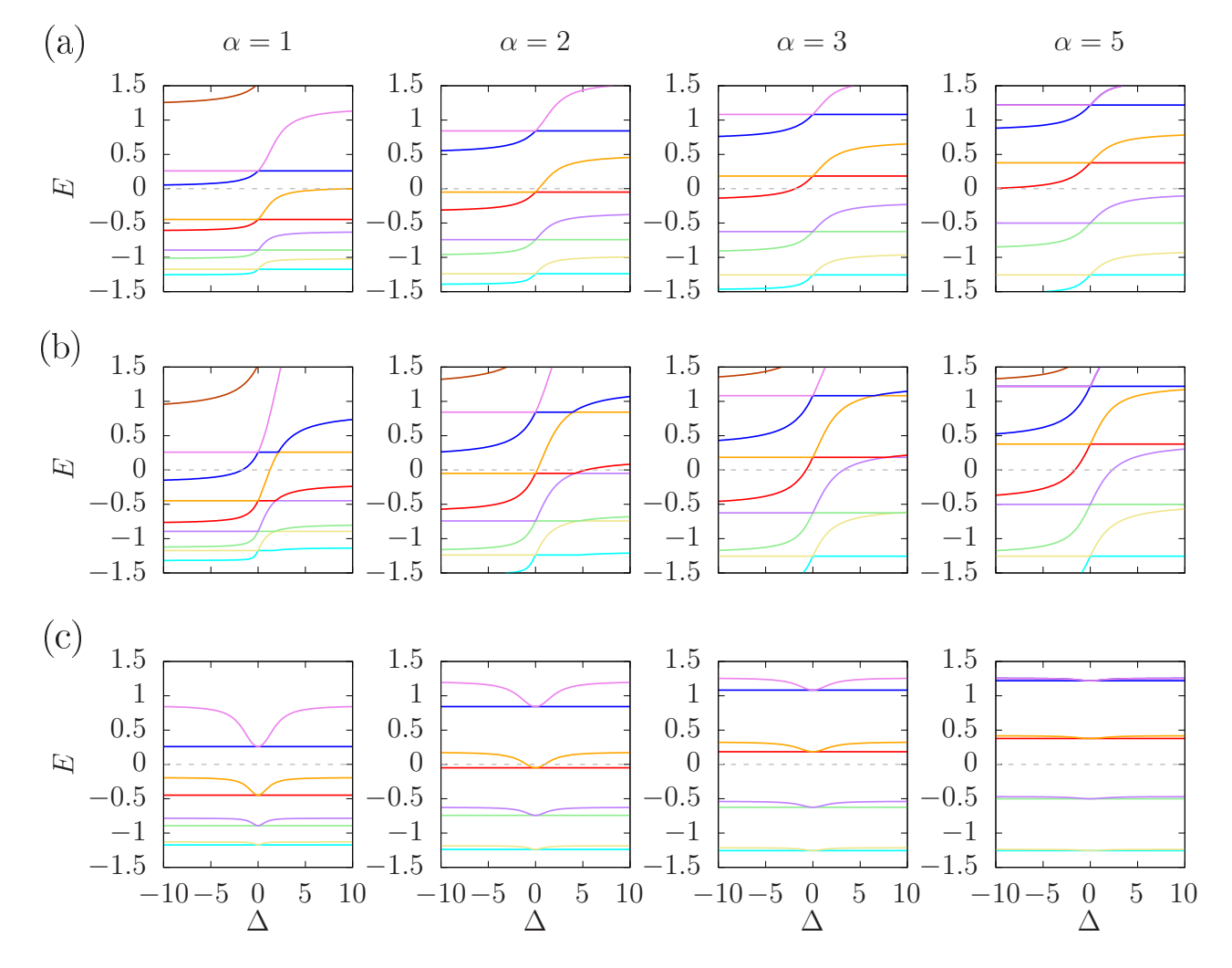


Figure 7: Numerical results for the spectrum of the long range XY model in the ring in presence of localized detunings (2a). Only close to zero energies are reported. The plot is organized in three panels: panel (a) reports results in presence of a single detuning, panel (b) reports results in presence of two equal detunings and panel (c) reports results in presence of two opposite detunings. For each panels we show results for $\alpha = 1, 2, 3, 5$. The number of sites is $N_r = 14$ and $J_{nn} = 1$.

 $\alpha = 2$.

It is safe to assume that the presence of the resonances strongly depends also on the number of atoms in the ring. The presence of size dependent resonance location can be immediately deduced from the perturbative results obtained in the previous section. Indeed, the unperturbed energy is $E_k^{(0)} = 2J\cos k$ where $k \sim 1/N_r$ and the first order shifts are directly proportional to Δ/N_r . In presence of long range hoppings we do not have access to exact spectrum of the Hamiltonian, however, at least for finite value of N_r we can analyze how the resonance position moves increasing the size. To be more precise, we consider the case of single barrier and plot the crossing states in function of Δ . Here, for crossing states we mean the states that cross the zero energy level in the interval $\Delta \in [-10, 0]$.

Figure 8 reports them and the first order linear corrections $E^{(0)} + 2\Delta/N_r$, where we extracted $E^{(0)}$ from numerical data and assumed that the first order perturbative shift is unchanged with respect to the nearest neighbor case. We immediately observe that for small values of Δ the linear shift keeps working well; indeed, increasing the size of the system, the slope of the shift is smaller. Moreover, the energy $E^{(0)}$ is smaller increasing the size and this makes the resonance position located at smaller values of $|\Delta|$ for bigger values of the size. Finally, we observe that

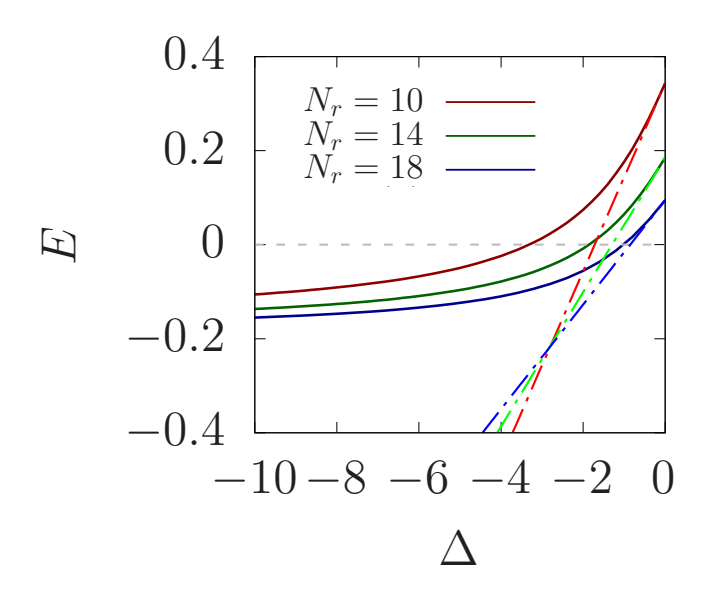


Figure 8: Crossing energy states in presence of a single barrier located at $j_0 = \lceil N_r/4 \rceil$ for three different values of the number of atoms in the ring N_r . The solid lines refers to numerical values of the energy for $N_r = 10$ (dark red), $N_r = 14$ (dark green) and $N_r = 18$ (dark blue). The dashed blue, green and blue lines refers to first perturbative order corrections $E^{(0)} + 2\Delta/N_r$ for respectively $N_r = 10, 14, 18$. In all the three cases $\alpha = 3$ and the parameters are set in such a way that $J_{nn} = 1$.

already for $N_r = 18$ the position of the resonance can be qualitatively estimated from the linear shift as $\Delta_{res} \approx -E^{(0)}N_r/2$, since it is located at a relatively small value of the detuning.

Appendix C Dynamics in absence of detunings

Here we analyze the dynamics of the system in absence of any type of detuning. We expect to find a non trivial dynamics also in absence of it; due to the geometry of the system, the excitation that travels along the system is subject to many scattering and splitting events. To have an idea of the complexity of the dynamics, let us consider an excitation subject only to nearest neighbor hopping that travels in the system starting from the source. The excitation moves from the source to the nearest site on the ring. The coupling between source and ring is smaller compared to the intra-ring one, thus, once a small excitation fraction reaches the ring, it is quickly split in the two arms of the ring. The splitted excitation fractions travel in the two arms of the ring and meet at the end of them, before the drain. Here, they scatter, a part of the excitation hops to the drain, the rest continues its dynamics in the arms of the ring. During a long time evolution a lot of scattering events occur and the dynamics will result complex and not intuitively easily to describe.

Figure 9 reports the population dynamics of the drain for different values of the inverse hopping range α . we consider $\alpha = 1$, $\alpha = 3$, nearest neighbor limit and the particular value of α for which, in absence of detuning, the ring presents zero energy levels resonant with the initial state. For instance, from Fig.7 we can observe that for N = 16 the particular α_{res} value is near to 2. Indeed, we find $\alpha_{res} = 2.168$; the other α_{res} values are reported in the Fig.9 labels. We observe how the drain population oscillates quite regularly except in the α_{res} case; the ring becomes is well populated and the oscillations are extremely irregular. For the other cases the ring is weakly populated, see Figs.2,3,4, thus it is important to follow the behavior of the drain density.

The latter is characterized by small frequency oscillations with big amplitude modulated by fast oscillations with small amplitude. In nearest neighbor limit, the two frequencies can be

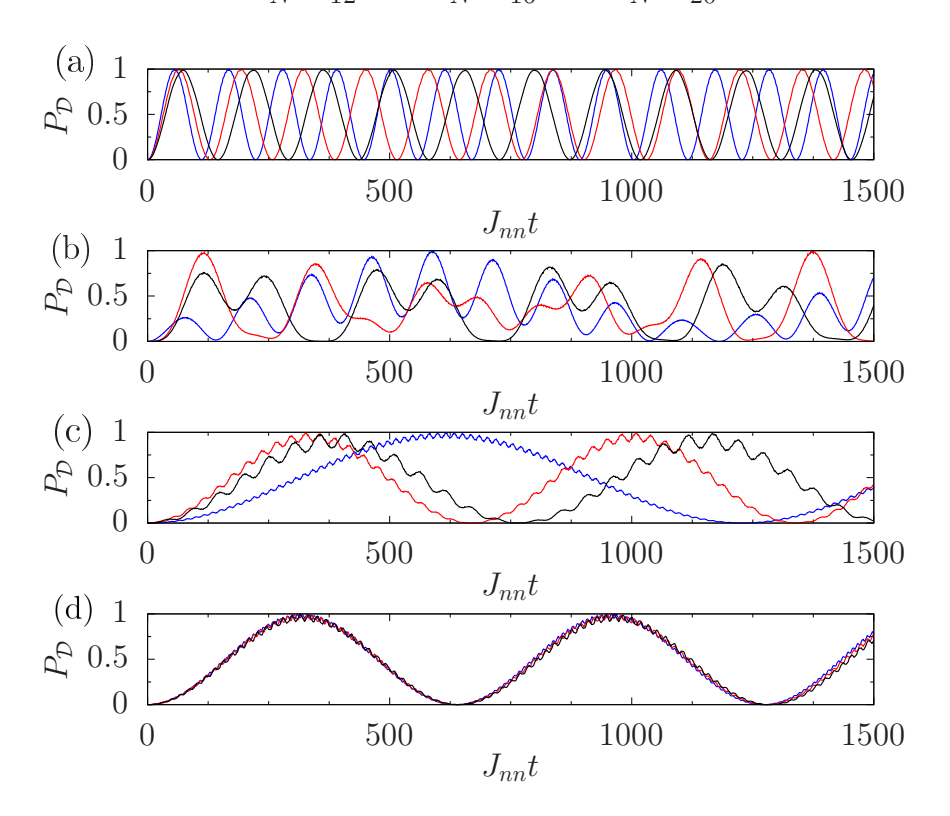


Figure 9: Dynamics of the drain population in absence of detunings in the ring. Results are reported for three different values of the size of the system: N=12 (blue), N=16 (red) and N=20 (black). The four panels refers to different values of the inverse hopping range: $\alpha=1$ in panel (a), $\alpha=3$ in panel (b), nearest neighbor in panel (d). Panel (b) shows the dynamics for the values of the inverse hopping range for which the ring presents zero energy levels in absence of detunings. These values are $\alpha_{res}=1.731$ (N=12), $\alpha_{res}=2.168$ (N=16), $\alpha_{res}=2.508$ (N=20). Leads and ring are weakly coupled $K_{nn}/J_{nn}=0.1$.

evaluated analytically [10]

$$\frac{\omega_{\pm}}{J_{nn}} = \pm \frac{N_r}{\delta} \frac{8 + \tilde{K}_{nn}^2 N_r - 2\tilde{K}_{nn}^2 \delta}{4\tilde{K}_{nn}^2 \delta^2 - N_r (8 + \tilde{K}_{nn}^2 N_r)} + \sqrt{\left(\frac{N_r}{\delta} \frac{8 + \tilde{K}_{nn}^2 N_r - 2\tilde{K}_{nn}^2 \delta}{4\tilde{K}_{nn}^2 \delta^2 - N_r (8 + \tilde{K}_{nn}^2 N_r)}\right)^2 + \frac{N_r}{\delta} \frac{8\tilde{K}_{nn}^2}{8N_r + \tilde{K}_{nn}^2 (N_r^2 - 4\delta^2)}}$$
(26)

where $\tilde{K}_{nn} = K_{nn}/J_{nn}$ and $\delta = \csc(\pi/N_r)$. From the numerical computation we can observe that the frequencies are weakly dependent on the size of the system. The non trivial form of the frequencies confirms how the dynamics is complex.

Surprisingly, for $\alpha=3$ the dynamics changes a lot with respect to the nearest neighbor limit. One of the crucial differences, is that here the leads are strongly connected with a plethora of sites near to the N_r and $N_r/2$, not just with one site. The first counter-intuitive result is the slow down of the dynamics with respect to the nearest neighbor case. The presence of hoppings does not cause a faster transport of the excitation from one site to the other. Secondly, the transport is slower for N=12, while N=16 is the faster case. Thus, a smaller size does not correspond to faster dynamics. Lastly, the case $\alpha=1$ is the most intuitive one. The hopping range is sufficiently large to avoid complex internal effects in the ring. The oscillation are faster

with respect to all the other case considered with smaller hopping range; moreover, increasing the size of the system it becomes slower.

Thus, the dynamics can result complex and nonintuitional also in absence of detunings barriers in the system, in particular, the Rydberg limit $\alpha = 3$ presents interesting features due to the complex dynamics that takes place in the ring.

Appendix D Information on the dynamics from the complete spectrum

In B we showed that important information on the dynamics can be extracted from the bare ring Hamiltonian, assuming that the ring and the leads are weakly coupled. Here, we focus our attention on the complete Hamiltonian, describing how the resonances manifest themselves on the state population and how the transport nature is modified and damaged from strong coupling and disorder.

D.1 Full Hamiltonian eigenstate nature

In the one excitation sector, a generic eigenstate of the Hamiltonian can be written in the computational basis as

$$|E_n\rangle = c_S^{(n)}|S\rangle + |R\rangle + c_D^{(n)}|D\rangle$$
 (27)

where $|\mathcal{S}\rangle = |\uparrow\rangle_{\mathcal{S}} \otimes |\downarrow, ..., \downarrow\rangle_{\mathcal{R}} \otimes |\downarrow\rangle_{\mathcal{D}}$, $|\mathcal{R}\rangle = \sum_{j\in\mathcal{R}} c_j^{(n)} |\downarrow\rangle_{\mathcal{S}} \otimes |\downarrow, ..., \uparrow_j, ..., \downarrow\rangle_{\mathcal{R}} \otimes |\downarrow\rangle_{\mathcal{D}}$ and $|\mathcal{D}\rangle = |\downarrow\rangle_{\mathcal{S}} \otimes |\downarrow, ..., \downarrow\rangle_{\mathcal{R}} \otimes |\uparrow\rangle_{\mathcal{D}}$. In absence of resonances, it is safe to assume that the leads and the ring degrees of freedom are separated. Thus, we group the states of the Hamiltonian in three classes: $\{|E_{n_l}\rangle, |E_{n_r}\rangle, |E_{n_l}\rangle\}$ are the states in which all the excitations are in the leads, $|E_{n_r}\rangle$ are the states in which only the ring is populated, and $|E_{n_{lr}}\rangle$ are the states in which the population is distributed between ring and leads; the labels satisfy the relation $n_l + n_r + n_{lr} = N$. Since the initial state of our protocol is $|\psi(0)\rangle = |\mathcal{S}\rangle$, the states $|E_{n_r}\rangle$ will not contribute to the dynamics; thus, the generic time evolved state can be written as

$$|\psi(t)\rangle = \sum_{n_l} e^{-iE_{n_l}t} \langle E_{n_l}|\mathcal{S}\rangle |E_{n_l}\rangle + \sum_{n_{lr}} e^{-iE_{n_{lr}}t} \langle E_{n_{lr}}|\mathcal{S}\rangle |E_{n_{lr}}\rangle.$$
(28)

Moreover, if the Hamiltonian spectrum does not contain uniform states $|E_{n_{lr}}\rangle$, the dynamics is dominated by the leads states $|E_{n_l}\rangle = c_{\mathcal{S}}^{(n_l)} |\mathcal{S}\rangle + c_{\mathcal{D}}^{(n_l)} |\mathcal{D}\rangle$ and will result in oscillations between source and drain of the form

$$|\psi(t)\rangle = \sum_{n_l} e^{-iE_{n_l}t} \left(c_{\mathcal{S}}^{(n_l)} \right)^* \left[c_{\mathcal{S}}^{(n_l)} |\mathcal{S}\rangle + c_{\mathcal{D}}^{(n_l)} |\mathcal{D}\rangle \right]. \tag{29}$$

The value of the lead state energies and their coefficients is fundamental to have information on the source-drain oscillation frequency and amplitude. On the other hand, the ring becomes populated only when the Hamiltonian has $|E_{n_{lr}}\rangle$ states. Thus, we expect to observe states $|E_{n_{lr}}\rangle$ in correspondence of the resonances.

In this section, we focus our attention on the eigenstate population $P_j^{(n)} = \langle E_n | \hat{n}_j | E_n \rangle$, we compute it for source, ring and drain in the whole spectrum. Figure 10 reports the behavior of the eigenstate populations in leads and ring for three different values of the size of the system, the inverse hopping range is $\alpha = 3$ and only one localized barrier at $j_0 = \lceil N_r/4 \rceil$ is taken into account. We immediately observe that the majority of the states of the system are ring states for which $P_{\mathcal{R}}^{(n)} \approx 1$ and $P_{\mathcal{S},\mathcal{D}}^{(n)} \approx 0$, they do not contribute to the dynamics if the system is initialized in $|S\rangle$.

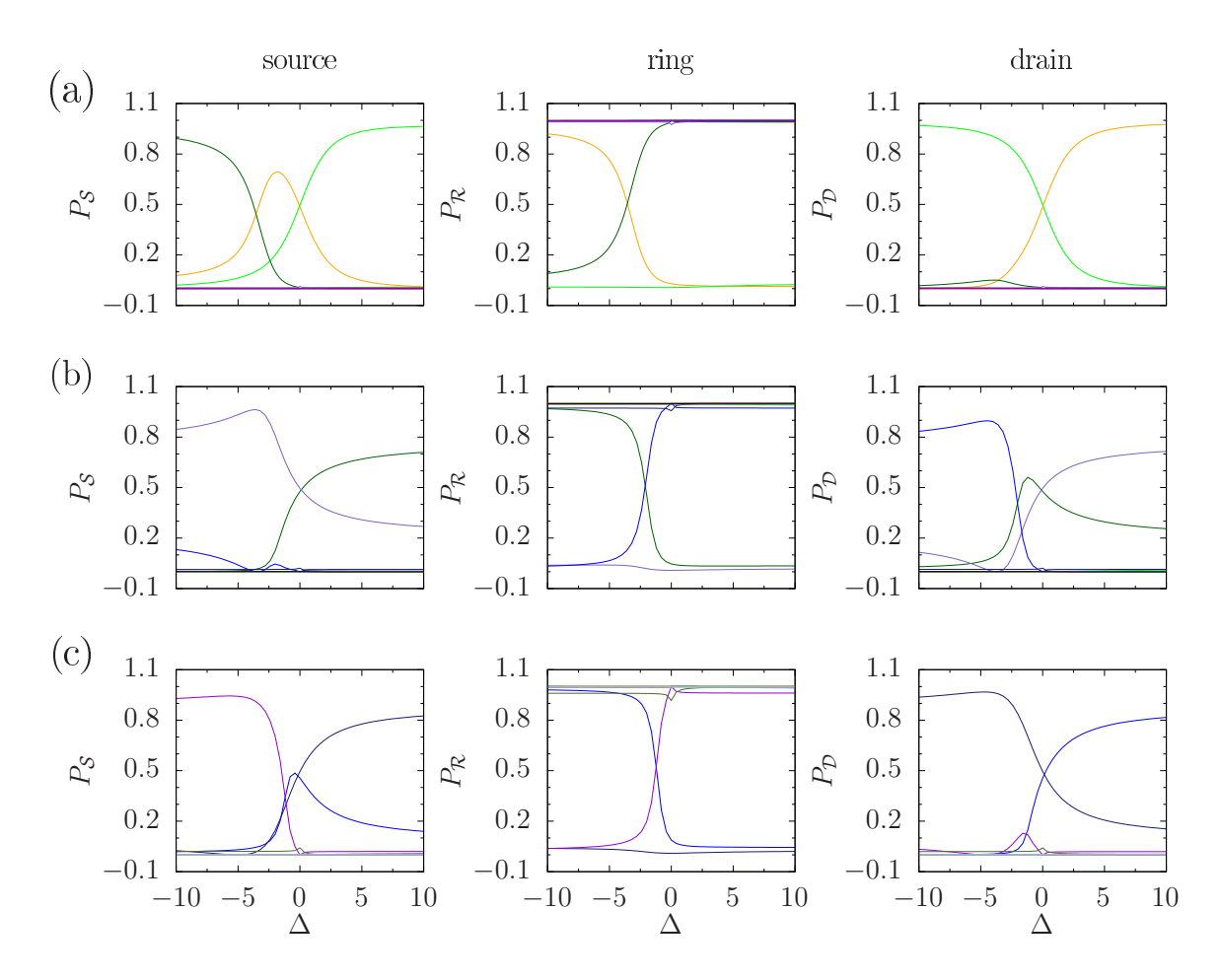


Figure 10: Source, ring and drain population from left to right in the spectrum for three different values of the size $N = N_r + 2$: N = 12 (panel (a)), N = 16 (panel (b)) and N = 20 (panel (c)). Most of the states are approximately ring states, meaning that their $P_{\mathcal{R}}^{(n)} \approx 1$. For each N only three states are not ring states: for N = 12 the 5-th, 6-th and 7-th (orange, green and dark green) excited states, for N = 16 the 7-th, 8-th and 9-th (dark green, purple and blue) excited states, for N = 20 the 9-th, 10-th and 11-th (blue, dark blue and violet) excited states. In all the three plots the parameters are set in such a way that $J_{nn} = 1$ and $K_{nn} = 0.1$, $\alpha = 3$. Only one barrier is taken into account.

From a comparison between Fig. 8 and Fig. 10 we observe that in correspondence of the resonance the ring population is 1/2 for two states of the spectrum, the excitation is equally distributed between ring and leads and this will result in a filling of the ring during the dynamics. Far from resonance, the Hamiltonian states are approximately ring or leads states with $P_{\mathcal{R}}^{(n)} \approx 0,1$; thus, the dynamics in leads states and will result in coherent oscillations between source and drain. Let us observe that leads states possess $P_{\mathcal{L}}^{(n)} = P_{\mathcal{S}}^{(n)} + P_{\mathcal{D}}^{(n)} = 1$, therefore, the nature of the

Let us observe that leads states possess $P_{\mathcal{L}}^{(n)} = P_{\mathcal{S}}^{(n)} + P_{\mathcal{D}}^{(n)} = 1$, therefore, the nature of the dynamics strongly depends on the source and drain population of the states. In particular, for $\Delta < \Delta_{res}$ there are source localized states, meaning states in which the source population is dominant an all the others. In absence of uniform states, the dynamics follows Eq. (29), that results in $|\psi(t)\rangle \approx e^{i\phi} |\mathcal{S}\rangle$ if there is a dominant localized source state. Thus, for $\Delta < \Delta_{res}$ the excitation remains localized in the source or at most a small fraction of it moves to the drain. The value of the population shows an irregular dependence on the size, the position of the resonance is size dependent and various finite size effects comes into play. Far from resonance, the size dependence is not regular, the source and drain populations follows different behaviors without a well defined dependence on the size. Thus, for each value of the size there is a resonance, but the dynamics far from the resonance strongly depends on N.

D.2 Eigenstate leads population for different leads-ring coupling

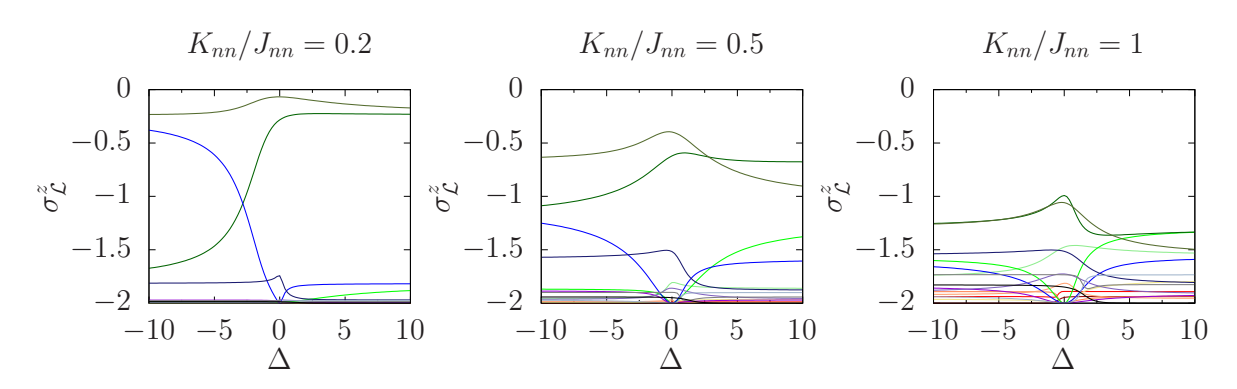


Figure 11: Leads magnetization in the spectrum in function of the barrier height Δ for different leadsring couplings K_{nn}/J_{nn} . $J_{nn}=1$ is fixed and K_{nn} is changed. $N_r=14$ and $\alpha=3$ are considered. The ring contains a single barrier localized in $\lceil N_r/4 \rceil$.

In the previous subsection we analyzed the full spectrum populations in the weak coupling regime. Here, we study it far from the weak coupling regime. We study the system in terms of leads population, in particular we analyze the leads magnetization that is directly related to leads and ring populations

$$\hat{\sigma}_{\mathcal{L}}^{z} = \hat{\sigma}_{\mathcal{S}}^{z} + \hat{\sigma}_{\mathcal{D}}^{z} = 2\left(\hat{n}_{\mathcal{L}} - \hat{1}\right) = -2\hat{n}_{\mathcal{R}}.$$
(30)

This means that leads and ring states have respectively $\langle \hat{\sigma}_{\mathcal{L}}^z \rangle = 0, -2.$

We are always focused on the Rydberg case $\alpha=3$, Fig. 11 reports the leads magnetization for three different values of the leads-ring coupling. Increasing the coupling the population of the eigentstates changes drastically. For small coupling only three states behave similarly to $|E_{n_{rl}}\rangle$ states around the resonance point, the states are the 7-th, 8-th and 9-th excited states. Increasing K_{nn}/J_{nn} , both $|E_{n_r}\rangle$ and $|E_{n_l}\rangle$ states become $|E_{n_{rl}}\rangle$ states. The spectrum is not anymore separated in well defined classes, this will result in a dynamics that is not characterized by coherent source-drain oscillation, but the ring will be populated not only for specific Δ values. Thus, the transport will not be anymore controllable tuning Δ .

D.3 Robustness against noise

Here we study the robustness of the results under the presence of disorder. In particular, we work with the impurity Hamiltonian

$$\hat{\mathcal{H}}_{imp} = \sum_{j \in \mathcal{R}} \Delta_j \hat{n}_j \tag{31}$$

where Δ_j is randomly extracted in the interval $[-\epsilon, +\epsilon]$ for each j except for $j = \lceil N_r/4 \rceil$ in which Δ_j belongs to the interval $[\Delta - \epsilon, \Delta + \epsilon]$. Therefore, it corresponds to the case of the single localized barrier in presence of noise. We study the effect of disorder on the leads population for $N_{rea} = 100$ disorder realizations in the single barrier case for N = 12 and $\alpha = 3$. We report the behavior of the expectation value

$$\overline{\langle E_n | \hat{\sigma}_{\mathcal{L}}^z | E_n \rangle} = \frac{1}{N_{rea}} \sum_{\beta=1}^{N_{rea}} \langle E_n^{(\beta)} | \hat{\sigma}_{\mathcal{L}}^z | E_n^{(\beta)} \rangle \tag{32}$$

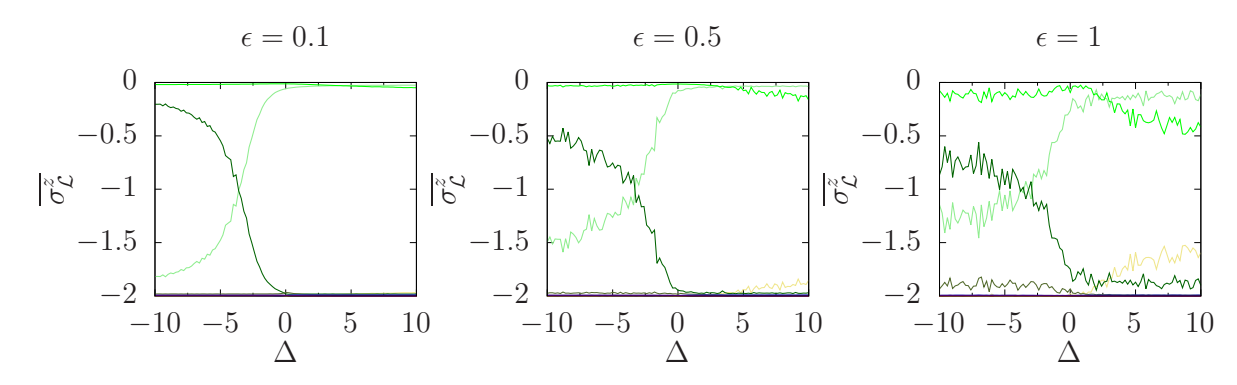


Figure 12: Leads magnetization in the spectrum in function of the barrier height Δ for different values of the disorder ϵ . $J_{nn}=1$ is fixed and $K_{nn}=0.1$ (weak coupling). $N_r=10$ and $\alpha=3$ are considered. The impurity Hamiltonian is 31. On the y axis it is reported the expectation value 32 for each n, it is reported as $\overline{\sigma_L^2}$ for sake of simplicity. $N_{rea}=100$ disorder realizations are taken into account.

which is the leads magnetization expectation value in the Hamiltonian spectrum averaged over many disorder realizations. $|E_n^{(\beta)}\rangle$ is the *n*-th eigenstate of the Hamiltonian for the β -th disorder realization. Fig.31 reports the behavior of the leads magnetization for different values of the disorder. We can observe how the presence of disorder can be dangerous for the population, indeed, for strong disorder ($\epsilon = 1$) ring and leads states can become $|E_{n_{lr}}\rangle$ states. However, a little amount of disorder ($\epsilon = 0.1$) does not modify the structure of the populations. In the intermediate case $\epsilon = 0.5$ the population behavior is slightly modified but keeps well the zero disorder structure with a resonance and a well defined separation between leads and ring states far from it.

Appendix E Phase difference dynamics

Here we provide more details on the phase effects that the presence of localized detunings generate. In the first part we show how the presence of a single localized detuning in the center of the chain of three atoms has significant effects on the phase associated to each site. For this reason, we suspect that a phase difference between two different paths with detuning located in different positions arises. Thus, in the second part of the section and in the main text we report the phase difference between two sites in the two arms in different conditions. We show that its dynamics is related to the population one.

E.1 Detuning-dependent phase difference in the three sites system

The presence of a localized detuning introduces a time dependent phase between different sites of the system. To see this, let us consider the simple three sites problem. We suppose to consider only nearest neighbor hopping, and put a localized detuning in the middle of the chain. As a first stage, we fix the detuning $\Delta=0$ and consider the three site Hamiltonian

$$\hat{\mathcal{H}}_{\text{hop}} = J \left(\hat{\sigma}_{1}^{+} \hat{\sigma}_{2}^{-} + \hat{\sigma}_{2}^{+} \hat{\sigma}_{3}^{-} + \text{H.c.} \right). \tag{33}$$

Supposing to consider the initial state $|\psi(0)\rangle = |\uparrow_1, \downarrow_2, \downarrow_3\rangle$ and evolve it through the Schrödinger equation. The resulting time-evolved state will be

$$|\psi(t)\rangle = \frac{1}{2} \left(\cos\left(\sqrt{2J}t\right) + 1 \right) |\uparrow_1, \downarrow_2, \downarrow_3\rangle + \frac{i}{\sqrt{2}} \sin\left(\sqrt{2J}t\right) |\downarrow_1, \uparrow_2, \downarrow_3\rangle + \frac{1}{2} \left(\cos\left(\sqrt{2J}t\right) - 1 \right) |\downarrow_1, \downarrow_2, \uparrow_3\rangle;$$
(34)

in absence of detuning, there is not a relative phase between the sites 1 and 3. In presence of a localized detuning, the Hamiltonian considered is $\hat{\mathcal{H}} = \hat{\mathcal{H}}_{hop} + \Delta \hat{n}_2$, the resulting time-evolved state will be

$$|\psi(t)\rangle = \left(\frac{e^{-i(\Delta - f(\Delta,J))t/2}}{\mathcal{N}_1^2} + \frac{e^{-i(\Delta + f(\Delta,J))t/2}}{\mathcal{N}_2^2} + \frac{1}{2}\right)|\uparrow_1,\downarrow_2,\downarrow_3\rangle + \left(\frac{(\Delta - f(\Delta,J))e^{-i(\Delta - f(\Delta,J))t/2}}{2J\mathcal{N}_1^2} + \frac{(\Delta + f(\Delta,J))e^{-i(\Delta + f(\Delta,J))t/2}}{2J\mathcal{N}_2^2}\right)|\downarrow_1,\uparrow_2,\downarrow_3\rangle + \left(\frac{e^{-i(\Delta - f(\Delta,J))t/2}}{\mathcal{N}_1^2} + \frac{e^{-i(\Delta + f(\Delta,J))t/2}}{\mathcal{N}_2^2} - \frac{1}{2}\right)|\downarrow_1,\downarrow_2,\uparrow_3\rangle$$
(35)

where $\mathcal{N}_1^2 = 2 + (\Delta - f(\Delta, J))^2 / 4J^2$, $\mathcal{N}_2^2 = 2 + (\Delta + f(\Delta, J))^2 / 4J^2$ and $f(\Delta, J) = \sqrt{\Delta^2 + 8J^2}$. In this way, the real and imaginary part of the $|\uparrow_1, \downarrow_2, \downarrow_3\rangle$ state will be

$$\operatorname{Re}\left(c_{\uparrow\downarrow\downarrow}(t)\right) = \frac{\cos\left((\Delta - f)t/2\right)}{\mathcal{N}_{1}^{2}} + \frac{\cos\left((\Delta + f)t/2\right)}{\mathcal{N}_{2}^{2}} + \frac{1}{2},\tag{36a}$$

$$\operatorname{Im}\left(c_{\uparrow\downarrow\downarrow}(t)\right) = -\frac{\sin\left((\Delta - f)t/2\right)}{\mathcal{N}_{1}^{2}} - \frac{\sin\left((\Delta + f)t/2\right)}{\mathcal{N}_{2}^{2}}.$$
 (36b)

The phase associated to the state is

$$\phi_{\uparrow\downarrow\downarrow}(t) = \tan^{-1} \left[\frac{\operatorname{Im} \left(c_{\uparrow\downarrow\downarrow}(t) \right)}{\operatorname{Re} \left(c_{\uparrow\downarrow\downarrow}(t) \right)} \right], \tag{37}$$

while the phase associated to the state $|\downarrow_1,\downarrow_2,\uparrow_3\rangle$ is

$$\phi_{\downarrow\downarrow\uparrow}(t) = \tan^{-1} \left[\frac{\operatorname{Im} \left(c_{\uparrow\downarrow\downarrow}(t) \right)}{\operatorname{Re} \left(c_{\uparrow\downarrow\downarrow}(t) \right) - 1} \right], \tag{38}$$

therefore, the two phases are different. In presence of detuning, a non-zero relative phase between the first and the last site of the chain is present. The difference with the zero detuning case is clear: the states $|\uparrow,\downarrow,\downarrow\rangle$ and $|\downarrow,\downarrow,\uparrow\rangle$ acquire a Δ -dependent phase, also the state $|\downarrow,\uparrow,\downarrow\rangle$ has a Δ -dependent phase differently from the zero detuning case in which it is fixed to $\pm \pi$.

E.2 Phase difference for different locations of detunings

If we consider two arms that differ from the detuning value, we expect to see a non-trivial phase difference between the sites of them. To formally evaluate the phase shift in the set-up considered in the main text, we write a generic time evolved states of the system in the position basis

$$|\psi(t)\rangle = c_{\mathcal{S}}(t) |\mathcal{S}\rangle + \sum_{j \in \mathcal{R}} c_j(t) |\downarrow\rangle_{\mathcal{S}} \otimes |\downarrow, ..., \uparrow_j, ..., \downarrow\rangle_{\mathcal{R}} \otimes |\downarrow\rangle_{\mathcal{D}} + c_{\mathcal{D}}(t) |\mathcal{D}\rangle,$$
(39)

and we observe that the two body correlator

$$\langle \hat{\sigma}_i^+ \hat{\sigma}_j^- \rangle = c_i^*(t)c_j(t) = |c_i(t)||c_j(t)||e^{i(\phi_j(t) - \phi_i(t))}$$
(40)

is directly related to the phase shift. Thus, the phase difference between the two sites i and j is accessible through $\delta\phi(t)=\phi_j(t)-\phi_i(t)=\arg\left(\langle\hat{\sigma}_i^+\hat{\sigma}_j^-\rangle\right)$. We can fix $i=N_r/2-1$ and

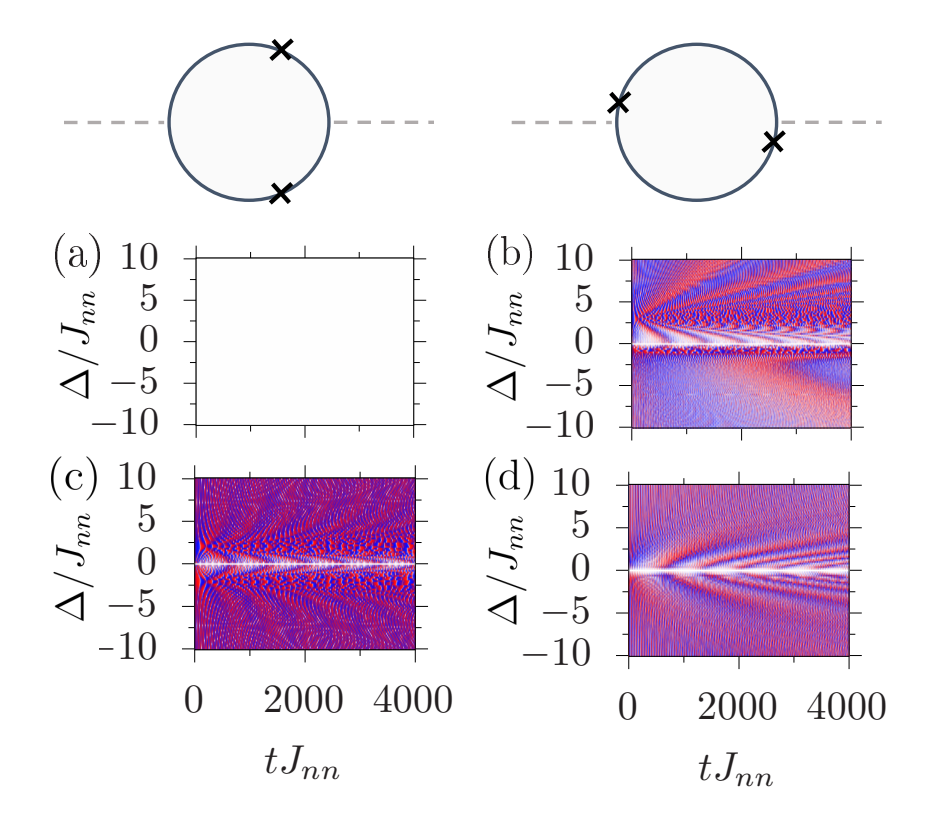


Figure 13: Phase difference $\delta \phi$ in function of detuning and time. Panels (a,c): phase difference for two equal (a) and opposite (c) detunings located at $j_A = \lceil N_r/4 \rceil$ and $j_B = \lceil 3N_r/4 \rceil - 1$ as in the top left sketch. Panels (b,d): phase difference for two equal (b) and opposite (d) detunings located at $j_A = 1$ and $j_B = N_r/2 + 1$ as in the top right sketch. The hopping range is fixed to $\alpha = 3$, $K_{nn}/J_{nn} = 0.1$

 $j = N_r/2 + 1$ in order to have information on the difference between the phases accumulated by excitation fractions crossing the two arms of the ring. Figures 2, 3, and 4 report the phase difference dynamics and detuning dependence for the configurations shown in Fig.1 showing its relation with the population dynamics. Here, we show the phase difference for alternative choices of the detunings location in the Rydberg case $\alpha = 3$.

We immediately observe that when the two detunigs have the same sign and the detuning locations are symmetric with respect to the leads [Fig. 13(a)], the phase difference is zero everywhere. Indeed, due to the symmetry of the system, the excitation acquires the same phase in the two arms. Differently, if the detunings are opposite, strong phase difference oscillations appear in such a way that it is never zero except in $\Delta = 0$ [Fig. 13(c)]. Figure 13(b,d) show the phase difference in a situation in which the distance between the detunings is the same as the one considered in the main text, meaning $j_B - j_A = N_r/2$, but they are located in different positions. As in the main text case, the equal barrier case presents two resonances for Δ_{red} analogous to those considered in the main text configuration, they are easily recognizable by fast phase difference oscillations. However, far from resonance, the dynamics is different and strongly depends on the the barrier location. The same applies to the opposite barrier case, there is no resonance but the nature of the oscillation is different.

Appendix F Chain

In this section we consider an analogous situation to those considered in the main text in which the channel is a chain of atoms. Thus, the only difference with the model considered in the main text is a new definition of the distances

$$d_{ij} = a|i-j|, \quad d_{\mathcal{SD}} = d_{\mathcal{SR}} + (N_c - 1)a + d_{\mathcal{DR}},$$

$$d_{\mathcal{S},j} = d_{\mathcal{SR}} + a(j-1), \quad d_{\mathcal{D},j} = d_{\mathcal{DR}} + a(N_c - j);$$
(41)

a is the lattice spacing in the chain, d_{SR} and d_{DR} are the distances between leads and chain, $N_c = N - 2$ is the number of atoms in the channel. The sites are labeled in such a way that j = 1 is the site connected to the source and $j = N_c$ is the site connected to the drain.

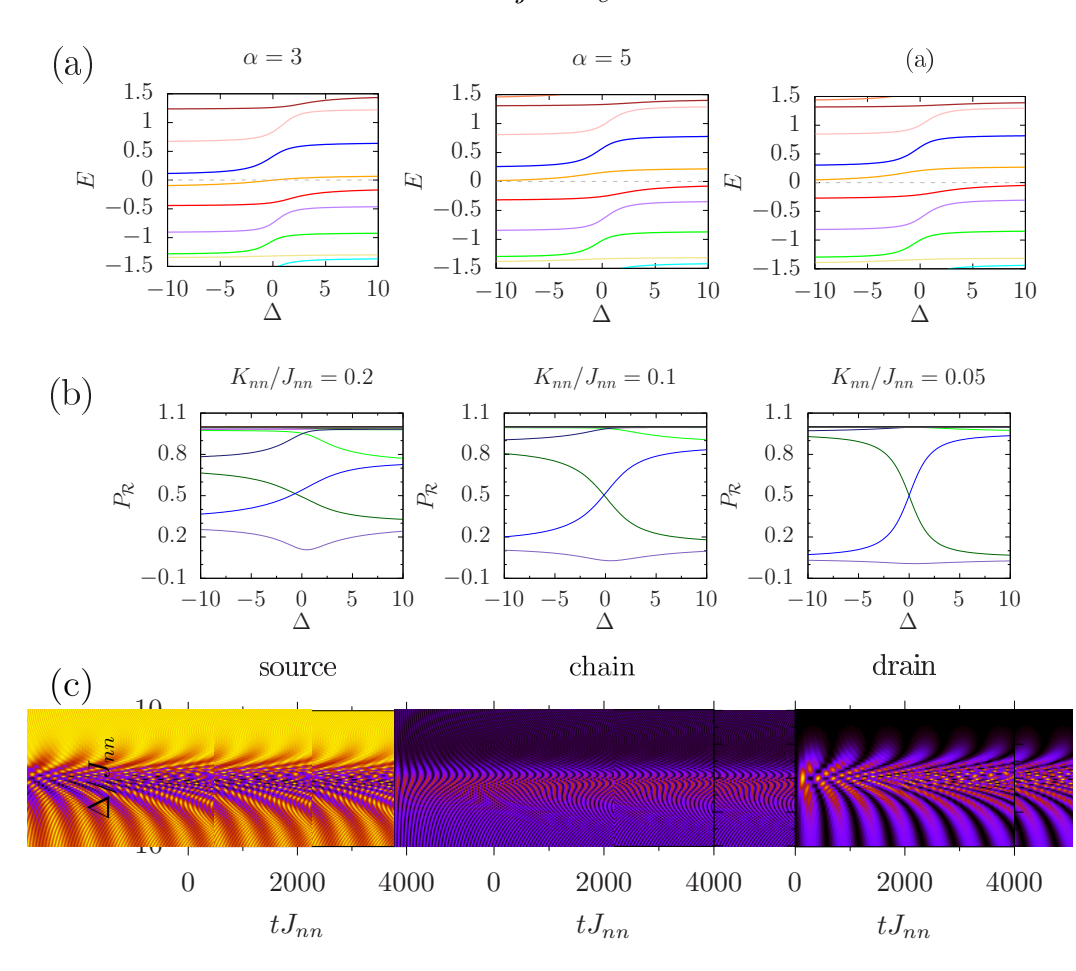


Figure 14: (a) Uncoupled spectrum close to zero energy, from left to right: $\alpha = 3$, $\alpha = 5$, $\alpha \to \infty$ which is the nearest neighbor limit; $J_{nn} = 1$ and $N_c = 14$. (b) Ring populations in the complete spectrum for different values of the ring-leads coupling K_{nn}/J_{nn} ; $\alpha = 3$, $J_{nn} = 1$ and $N_c = 14$. (c) Dynamics of the source, chain and drain populations (from left to right) for different values of the detuning; the leads-chain coupling is weak $K_{nn} = 0.05$, $J_{nn} = 1$, the inverse hopping range and the number of atoms are $\alpha = 3$ and $N_c = 14$. In all the three panels a single detuning located at $j_0 = \lceil N_c/4 \rceil$ is considered.

In the nearest neighbor limit the channel Hamiltonian in absence of detunings can be diagonalized passing first through a Jordan Wigner transformation and then rotating appropriately the creation and destruction operators. The unperturbed Hamiltonian turns out to be [53]

$$\hat{\mathcal{H}}_0 = \sum_{n=1}^{N_c} E_n^{(0)} \hat{d}_n^{\dagger} \hat{d}_n, \quad E_n^{(0)} = 2J \cos\left(\frac{\pi n}{N_c + 1}\right), \quad \hat{c}_j = \sqrt{\frac{2}{N_c + 1}} \sum_{n=1}^{N_c} \sin\left(\frac{\pi j n}{N_c + 1}\right) \hat{d}_n. \quad (42)$$

In this case the spectrum is not degenerate, thus the barrier will simply shift the energy levels without splitting any degeneracy. In the case of non-degenerate spectrum the first order correction in presence of a single detuning located at the position j_0 can be straightforwardly

calculated

$$\Delta E_n^{(1)} = \Delta \langle n | \hat{n}_{j_0} | n \rangle = \frac{2\Delta}{N_c + 1} \sin^2 \left(\frac{\pi n j_0}{N_c + 1} \right). \tag{43}$$

We are interested on the role of the long range hopping. Fig. 14(a) reports the energy spectrum of the uncoupled chain Hamiltonian near to the zero energy value for different values of α . For $\Delta=0$ and in the nearest neighbor case, the spectrum is symmetric with respect to E=0, then a linear shift of the levels is caused by Δ . As in the ring case, with a single detuning the shift is not sufficient to have a resonance at zero energy in the detuning interval considered. Increasing the hopping range and so decreasing α , the levels are basically shifted downwards in terms of energy. For this reason, for finite α it is possible that resonances appear. For $\alpha=3$, we observe a resonance with the zero energy state at Δ around zero. The presence of a resonance will allow us to state that the ring will be populated during the dynamics.

However, as observed previously, the presence of resonances is not sufficient to have complete information on the dynamics. It is also important to understand how the complete spectrum of leads and chain behaves in Δ . In Fig. 14(b) we show the ring population for three different values of the leads-chain coupling K_{nn}/J_{nn} . We can immediately observe that in this case also for $K_{nn}/J_{nn}=0.1$ ring and leads states are not well separated. In particular, far from resonance, many eigenstates are of the form $|E_{nl}\rangle$ and so the dynamics will not result in coherent oscillations between source and drain. For $K_{nn}/J_{nn}=0.05$ the separation is better defined for big values of Δ , while around the resonance the ring population is 1/2. Thus, we can conclude that to decouple leads and chain we need a bigger distances between them with respect to ring case.

Finally, Fig. 14(c) reports the dynamics of the source, chain and drain population for $K_{nn}/J_{nn} = 0.05$. In proximity of the resonance the ring is heavily populated to the disadvantage of the source. Increasing the value of the detuning and going far from resonance, the transport through the ring is reduced; however, the Δ -window in which the ring is populated and is not simply a narrow region as in the ring case.

References

- [1] CWJ Beenakker and Henk van Houten. Quantum transport in semiconductor nanostructures. In *Solid state physics*, volume 44, pages 1–228. Elsevier, 1991.
- [2] Ya M Blanter and Markus Büttiker. Shot noise in mesoscopic conductors. *Physics reports*, 336(1-2):1–166, 2000.
- [3] Supriyo Datta. Quantum transport: atom to transistor. Cambridge university press, 2005.
- [4] Yuli V Nazarov and Yaroslav M Blanter. Quantum transport: introduction to nanoscience. Cambridge university press, 2009.
- [5] AD Stone. Theory of coherent quantum transport. In *Physics of Nanostructures*, pages 65–100. Institute of Physics, 1992.
- [6] Chih-Chun Chien, Sebastiano Peotta, and Massimiliano Di Ventra. Quantum transport in ultracold atoms. *Nature Physics*, 11(12):998–1004, 2015.
- [7] David Stadler, Sebastian Krinner, Jakob Meineke, Jean-Philippe Brantut, and Tilman Esslinger. Observing the drop of resistance in the flow of a superfluid fermi gas. *Nature*, 491(7426):736, 2012.

- [8] Dominik Husmann, Shun Uchino, Sebastian Krinner, Martin Lebrat, Thierry Giamarchi, Tilman Esslinger, and Jean-Philippe Brantut. Connecting strongly correlated superfluids by a quantum point contact. *Science*, 350(6267):1498–1501, 2015.
- [9] Laura Corman, Philipp Fabritius, Samuel Häusler, Jeffrey Mohan, Lena H Dogra, Dominik Husmann, Martin Lebrat, and Tilman Esslinger. Quantized conductance through a dissipative atomic point contact. arXiv preprint arXiv:1907.06436, 2019.
- [10] Tobias Haug, Hermanni Heimonen, Rainer Dumke, Leong-Chuan Kwek, and Luigi Amico. Aharonov-bohm effect in mesoscopic bose-einstein condensates. *Physical Review A*, 100(4):041601, 2019.
- [11] Luigi Amico, Malcolm Boshier, Gerhard Birkl, Anna Minguzzi, Christian Miniatura, L-C Kwek, Davit Aghamalyan, Veronica Ahufinger, Dana Anderson, Natan Andrei, et al. Roadmap on atomtronics: State of the art and perspective. *AVS Quantum Science*, 3(3), 2021.
- [12] Luigi Amico, Dana Anderson, Malcolm Boshier, Jean-Philippe Brantut, Leong-Chuan Kwek, Anna Minguzzi, and Wolf von Klitzing. Colloquium: Atomtronic circuits: From many-body physics to quantum technologies. *Reviews of Modern Physics*, 94(4):041001, 2022.
- [13] M Büttiker, Y Imry, and M Ya Azbel. Quantum oscillations in one-dimensional normal-metal rings. *Physical Review A*, 30(4):1982, 1984.
- [14] Yuval Gefen, Yoseph Imry, and M Ya Azbel. Quantum oscillations and the aharonov-bohm effect for parallel resistors. *Physical review letters*, 52(2):129, 1984.
- [15] Sean Washburn and Richard A Webb. Aharonov-bohm effect in normal metal quantum coherence and transport. *Advances in Physics*, 35(4):375–422, 1986.
- [16] David J Griffiths. Ouantum mechanics. 2003.
- [17] C Ryu, PW Blackburn, AA Blinova, and MG Boshier. Experimental realization of josephson junctions for an atom squid. *Physical review letters*, 111(20):205301, 2013.
- [18] Changhyun Ryu, EC Samson, and Malcolm Geoffrey Boshier. Quantum interference of currents in an atomtronic squid. *Nature communications*, 11(1):3338, 2020.
- [19] Katarzyna A Krzyzanowska, Jorge Ferreras, Changhyun Ryu, Edward Carlo Samson, and Malcolm G Boshier. Matter-wave analog of a fiber-optic gyroscope. *Physical Review A*, 108(4):043305, 2023.
- [20] Brynle Barrett, Rémy Geiger, Indranil Dutta, Matthieu Meunier, Benjamin Canuel, Alexandre Gauguet, Philippe Bouyer, and Arnaud Landragin. The sagnac effect: 20 years of development in matter-wave interferometry. *Comptes Rendus Physique*, 15(10):875–883, 2014.
- [21] Rainer Blatt and Christian F Roos. Quantum simulations with trapped ions. *Nature Physics*, 8(4):277–284, 2012.
- [22] Christopher Monroe, Wes C Campbell, L-M Duan, Z-X Gong, Alexey V Gorshkov, Paul W Hess, Rajibul Islam, Kihwan Kim, Norbert M Linke, Guido Pagano, et al. Programmable quantum simulations of spin systems with trapped ions. *Reviews of Modern Physics*, 93(2):025001, 2021.

- [23] Antoine Browaeys and Thierry Lahaye. Many-body physics with individually controlled rydberg atoms. *Nature Physics*, 16(2):132–142, 2020.
- [24] Hannes Bernien, Sylvain Schwartz, Alexander Keesling, Harry Levine, Ahmed Omran, Hannes Pichler, Soonwon Choi, Alexander S Zibrov, Manuel Endres, Markus Greiner, et al. Probing many-body dynamics on a 51-atom quantum simulator. *Nature*, 551(7682):579–584, 2017.
- [25] Daniel Barredo, Sylvain De Léséleuc, Vincent Lienhard, Thierry Lahaye, and Antoine Browaeys. An atom-by-atom assembler of defect-free arbitrary two-dimensional atomic arrays. *Science*, 354(6315):1021–1023, 2016.
- [26] Kai-Niklas Schymik, Vincent Lienhard, Daniel Barredo, Pascal Scholl, Hannah Williams, Antoine Browaeys, and Thierry Lahaye. Enhanced atom-by-atom assembly of arbitrary tweezer arrays. *Physical Review A*, 102(6):063107, 2020.
- [27] Gerhard Birkl, Sven Kassner, and Herbert Walther. Multiple-shell structures of laser-cooled 24mg+ ions in a quadrupole storage ring. *Nature*, 357(6376):310–313, 1992.
- [28] Dominik Kiesenhofer, Helene Hainzer, Artem Zhdanov, Philip C Holz, Matthias Bock, Tuomas Ollikainen, and Christian F Roos. Controlling two-dimensional coulomb crystals of more than 100 ions in a monolithic radio-frequency trap. *PRX Quantum*, 4(2):020317, 2023.
- [29] Christine Maier, Tiff Brydges, Petar Jurcevic, Nils Trautmann, Cornelius Hempel, Ben P Lanyon, Philipp Hauke, Rainer Blatt, and Christian F Roos. Environment-assisted quantum transport in a 10-qubit network. *Physical review letters*, 122(5):050501, 2019.
- [30] Daniel Barredo, Henning Labuhn, Sylvain Ravets, Thierry Lahaye, Antoine Browaeys, and Charles S Adams. Coherent excitation transfer in a spin chain of three rydberg atoms. *Physical review letters*, 114(11):113002, 2015.
- [31] Fan Yang, Shuo Yang, and Li You. Quantum transport of rydberg excitons with synthetic spin-exchange interactions. *Physical Review Letters*, 123(6):063001, 2019.
- [32] Iñigo Arrazola, Julen S Pedernales, Lucas Lamata, and Enrique Solano. Digital-analog quantum simulation of spin models in trapped ions. *Scientific reports*, 6(1):30534, 2016.
- [33] Philip Richerme, Zhe-Xuan Gong, Aaron Lee, Crystal Senko, Jacob Smith, Michael Foss-Feig, Spyridon Michalakis, Alexey V Gorshkov, and Christopher Monroe. Non-local propagation of correlations in quantum systems with long-range interactions. *Nature*, 511(7508):198–201, 2014.
- [34] Justin G Bohnet, Brian C Sawyer, Joseph W Britton, Michael L Wall, Ana Maria Rey, Michael Foss-Feig, and John J Bollinger. Quantum spin dynamics and entanglement generation with hundreds of trapped ions. *Science*, 352(6291):1297–1301, 2016.
- [35] Kenneth R Brown, Jungsang Kim, and Christopher Monroe. Co-designing a scalable quantum computer with trapped atomic ions. *npj Quantum Information*, 2(1):1–10, 2016.
- [36] Fereshteh Rajabi, Sainath Motlakunta, Chung-You Shih, Nikhil Kotibhaskar, Qudsia Quraishi, Ashok Ajoy, and Rajibul Islam. Dynamical hamiltonian engineering of 2d rectangular lattices in a one-dimensional ion chain. npj Quantum Information, 5(1):32, 2019.

- [37] Lucia Duca, Naoto Mizukami, Elia Perego, Massimo Inguscio, and Carlo Sias. Orientational melting in a mesoscopic system of charged particles. *Physical Review Letters*, 131(8):083602, 2023.
- [38] Joseph W Britton, Brian C Sawyer, Adam C Keith, C-C Joseph Wang, James K Freericks, Hermann Uys, Michael J Biercuk, and John J Bollinger. Engineered two-dimensional ising interactions in a trapped-ion quantum simulator with hundreds of spins. *Nature*, 484(7395):489–492, 2012.
- [39] Bryce Yoshimura, Marybeth Stork, Danilo Dadic, Wesley C Campbell, and James K Freericks. Creation of two-dimensional coulomb crystals of ions in oblate paul traps for quantum simulations. *EPJ Quantum Technology*, 2:1–17, 2015.
- [40] Philip Richerme. Two-dimensional ion crystals in radio-frequency traps for quantum simulation. *Physical Review A*, 94(3):032320, 2016.
- [41] Atsushi Noguchi, Yutaka Shikano, Kenji Toyoda, and Shinji Urabe. Aharonov-bohm effect in the tunnelling of a quantum rotor in a linear paul trap. *Nature communications*, 5(1):3868, 2014.
- [42] Hao-Kun Li, Erik Urban, Crystal Noel, Alexander Chuang, Yang Xia, Anthony Ransford, Boerge Hemmerling, Yuan Wang, Tongcang Li, Hartmut Häffner, et al. Realization of translational symmetry in trapped cold ion rings. *Physical review letters*, 118(5):053001, 2017.
- [43] Cheng Chen, Guillaume Bornet, Marcus Bintz, Gabriel Emperauger, Lucas Leclerc, Vincent S Liu, Pascal Scholl, Daniel Barredo, Johannes Hauschild, Shubhayu Chatterjee, et al. Continuous symmetry breaking in a two-dimensional rydberg array. *Nature*, 616(7958):691–695, 2023.
- [44] Guillaume Bornet, Gabriel Emperauger, Cheng Chen, Bingtian Ye, Maxwell Block, Marcus Bintz, Jamie A Boyd, Daniel Barredo, Tommaso Comparin, Fabio Mezzacapo, et al. Scalable spin squeezing in a dipolar rydberg atom array. arXiv preprint arXiv:2303.08053, 2023.
- [45] Vincent Lienhard, Pascal Scholl, Sebastian Weber, Daniel Barredo, Sylvain de Léséleuc, Rukmani Bai, Nicolai Lang, Michael Fleischhauer, Hans Peter Büchler, Thierry Lahaye, et al. Realization of a density-dependent peierls phase in a synthetic, spin-orbit coupled rydberg system. *Physical Review X*, 10(2):021031, 2020.
- [46] DV Averin and Yu V Nazarov. Virtual electron diffusion during quantum tunneling of the electric charge. *Physical Review Letters*, 65(19):2446, 1990.
- [47] TB Tran, IS Beloborodov, Jingshi Hu, XM Lin, TF Rosenbaum, and HM Jaeger. Sequential tunneling and inelastic cotunneling in nanoparticle arrays. *Physical Review B*, 78(7):075437, 2008.
- [48] Petar Jurcevic, Ben P Lanyon, Philipp Hauke, Cornelius Hempel, Peter Zoller, Rainer Blatt, and Christian F Roos. Quasiparticle engineering and entanglement propagation in a quantum many-body system. *Nature*, 511(7508):202–205, 2014.
- [49] Sebastian Krämer, David Plankensteiner, Laurin Ostermann, and Helmut Ritsch. Quantumoptics. jl: A julia framework for simulating open quantum systems. *Computer Physics Communications*, 227:109–116, 2018.

- [50] David J Griffiths and Darrell F Schroeter. *Introduction to quantum mechanics*. Cambridge university press, 2018.
- [51] Pascual Jordan and Eugene Paul Wigner. Über das paulische äquivalenzverbot. Springer, 1993.
- [52] Antonella De Pasquale and Paolo Facchi. XY model on the circle: Diagonalization, spectrum, and forerunners of the quantum phase transition. *Physical Review A*, 80(3):032102, 2009.
- [53] Suraj Hegde, Vasudha Shivamoggi, Smitha Vishveshwara, and Diptiman Sen. Quench dynamics and parity blocking in majorana wires. *New Journal of Physics*, 17(5):053036, 2015.